Research article

JHEP|Reports

Sex differences in murine MASH induced by a fructose-palmitate-cholesterol-enriched diet

Authors

Lakshmi Arivazhagan, Sofie Delbare, Robin A. Wilson, …, Edward A. Fisher, Neil D. Theise, Ann Marie Schmidt

Correspondence

annmarie.schmidt@nyulangone.org (A.M. Schmidt).

Graphical abstract

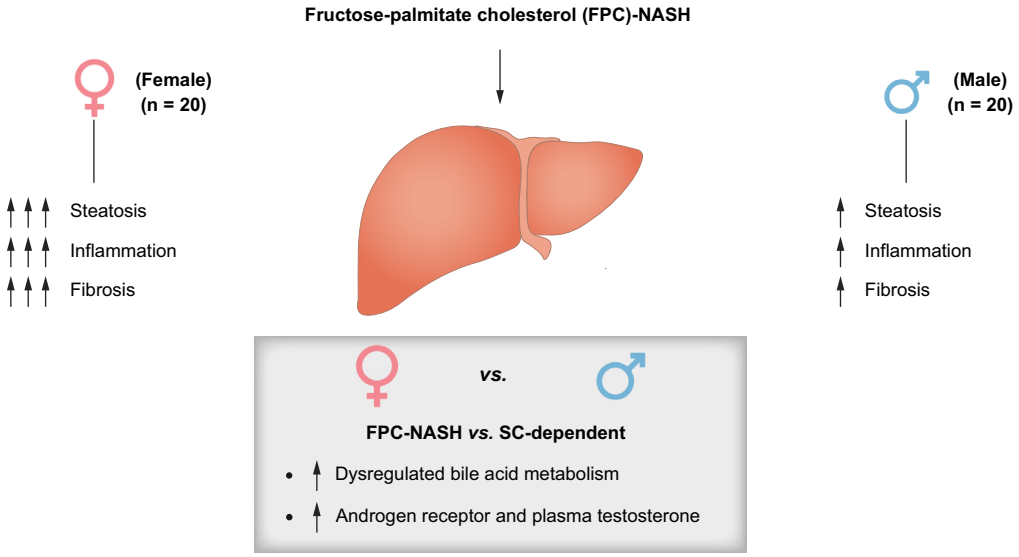

Highlights:

- Higher MASH scores are observed in the livers of female *vs.* male mice fed a NASH diet.
- Analyses reveal greater dysregulation of bile acid metabolism in female *vs.* male mice.
- Greater androgen receptor activity is observed in female *vs.* male mice.
- Many of these findings were recapitulated in human liver datasets of patients with MASH.

Impact and implications:

Despite the importance of metabolic dysfunction-associated steatohepatitis (MASH) in impairment of human health, the potential for and mechanisms of sex-dependent responses have yet to be well-studied, particularly with respect to the possible influence of high-fructose corn syrup additives to the diet, which has been linked to metabolic and hepatic disturbances. In a mouse model of fructose supplementation to a NASH diet, female mice displayed significantly higher MASH scores (steatosis, inflammation and fibrosis) compared to male mice. Single-nucleus RNA sequencing of livers revealed intrinsic, diet-dependent molecular disparities within sex, which were exaggerated when comparing female *vs.* male mice fed the fructose-containing NASH diet; many of these findings were recapitulated in human female *vs.* male patients with MASH. These results highlight potential mechanistic explanations and therapeutic targets for addressing sex differences and underscore the need to study both sexes in animal models and human MASH.

https://doi.org/10.1016/j.jhepr.2024.101222

 JHEP Reports, 2025, 7, 1–22

Research article

JHEP|Reports

Sex differences in murine MASH induced by a fructose-palmitate-cholesterol-enriched diet

Lakshmi Arivazhagan[1], Sofie Delbare[2], Robin A. Wilson[1], Michaele B. Manigrasso[1], Boyan Zhou[3], Henry H. Ruiz[1], Kaamashri Mangar[1], Ryoko Higa[1], Emily Brown[2], Huilin Li[3], Michael J. Garabedian[4], Ravichandran Ramasamy[1], Kathryn J. Moore[2], Edward A. Fisher[2], Neil D. Theise[5], Ann Marie Schmidt[1,*]

JHEP Reports **2025**. vol. 7 | 1–22

Background & Aims: Metabolic syndrome-associated steatotic liver disease (MASLD) and metabolic syndrome-associated steatohepatitis (MASH) have global prevalence rates exceeding 25% and 3-6%, respectively. The introduction of high-fructose corn syrup to the diet in the 1970s has been linked to metabolic and hepatic disturbances. Despite these associations, the potential for sex-dependent responses resulting from fructose-containing diets on MASLD/MASH has not been addressed.

Methods: Female and male C57BL/6J mice were fed a fructose-palmitate-cholesterol (FPC)-NASH diet *vs.* standard chow for 16 weeks (n = 40 mice). At sacrifice, plasma and liver were retrieved, the latter for single-nucleus RNA sequencing. Publicly available data sets of human male and female MASH liver were probed.

Results: The FPC-NASH diet-induced metabolic dysfunction in both female and male mice, with females exhibiting more severe hepatic steatosis (p = 0.0262), inflammation (p = 0.0206), and fibrosis (p <0.0001). Single-nucleus RNA sequencing revealed distinct sex-specific transcriptional profiles in hepatocytes and stellate cells responding to the FPC-NASH diet compared to the standard chow. In female mice, compared to males, pathways associated with lipid and metabolic processes in hepatocytes and cell-cell communication and adhesion in stellate cells were enriched. Metabolic flux analyses demonstrated reduced bile acid metabolism in female mice and human hepatocytes in FPC-NASH and MASH conditions, respectively, compared to their male counterparts.

Conclusions: Molecular profiling of hepatocytes and stellate cells in FPC-NASH diet-fed mice revealed significant sex differences mirrored in human MASH. The identification of intrinsic, within-sex, diet-dependent disparities underscores the critical need to include both male and female individuals in MAFLD/MASH studies and clinical trials.

Introduction

The worldwide prevalence of metabolic dysfunction-associated steatotic liver disease (MASLD) exceeds 25%[1] and that of the advanced form of disease manifesting with inflammation and cellular injury, metabolic dysfunction-associated steatohepatitis (MASH), is 3-6%.[2] MASLD/MASH is strongly associated with obesity, insulin resistance and type 2 diabetes; however, not all individuals with these metabolic disorders develop MASLD/MASH[2] and lean persons without metabolic dysfunction have been diagnosed with these disorders.[3]

Although younger patients diagnosed with MASH are predominantly males, the prevalence of MASH is higher in females after age 60 years.[4,5] A study from Japan reported higher rates of cirrhotic MASH in women (57%) than in men (43%).[5] Others reported that women aged 50 years or older with MASLD may be up to 1.2-fold more likely to develop MASH and progress to advanced fibrosis when compared to men of the same age.[6] A report from the US indicated that between 1999 and 2022, the age-adjusted MASLD-related mortality rate rose from 0.2 to 1.7 per 100,000.[7] Females demonstrated a steeper rise than males, 0.2-2 per 100,000 with an average annual percent change of 11.7% (p <0.001) *vs.* 0.2-1.3 per 100,000 and average annual percent change of 9.3% in males, respectively (p <0.001).[7] Hence, although the onset of MASLD may occur earlier in males *vs.* females, the severity of disease may be worse in women.[7,8]

From the 1970s, significant changes to the forms of carbohydrates in dietary food and beverages occurred[9,10] and the makers of soft drinks Coke and Pepsi largely replaced beet sugar with high-fructose corn syrup.[11] A report on the Framingham Heart Study cohorts published in 2015 indicated that sugar-sweetened beverage consumption was associated with higher odds ratio of fatty liver disease (p-trend 0.04), even after adjustment for age, sex, smoking, Framingham cohort, energy intake, alcohol, dietary fiber, fat (% energy), protein (% energy), diet soda intake and body mass index.[12] Furthermore, the consumption of sugar-sweetened beverages was positively associated with alanine aminotransferase (ALT) (p-trend 0.007);

* Corresponding author. Address: Diabetes Research Program, Department of Medicine, New York University Grossman School of Medicine Langone Health, New York, NY 10016, USA.
E-mail address: annmarie.schmidt@nyulangone.org (A.M. Schmidt).
https://doi.org/10.1016/j.jhepr.2024.101222

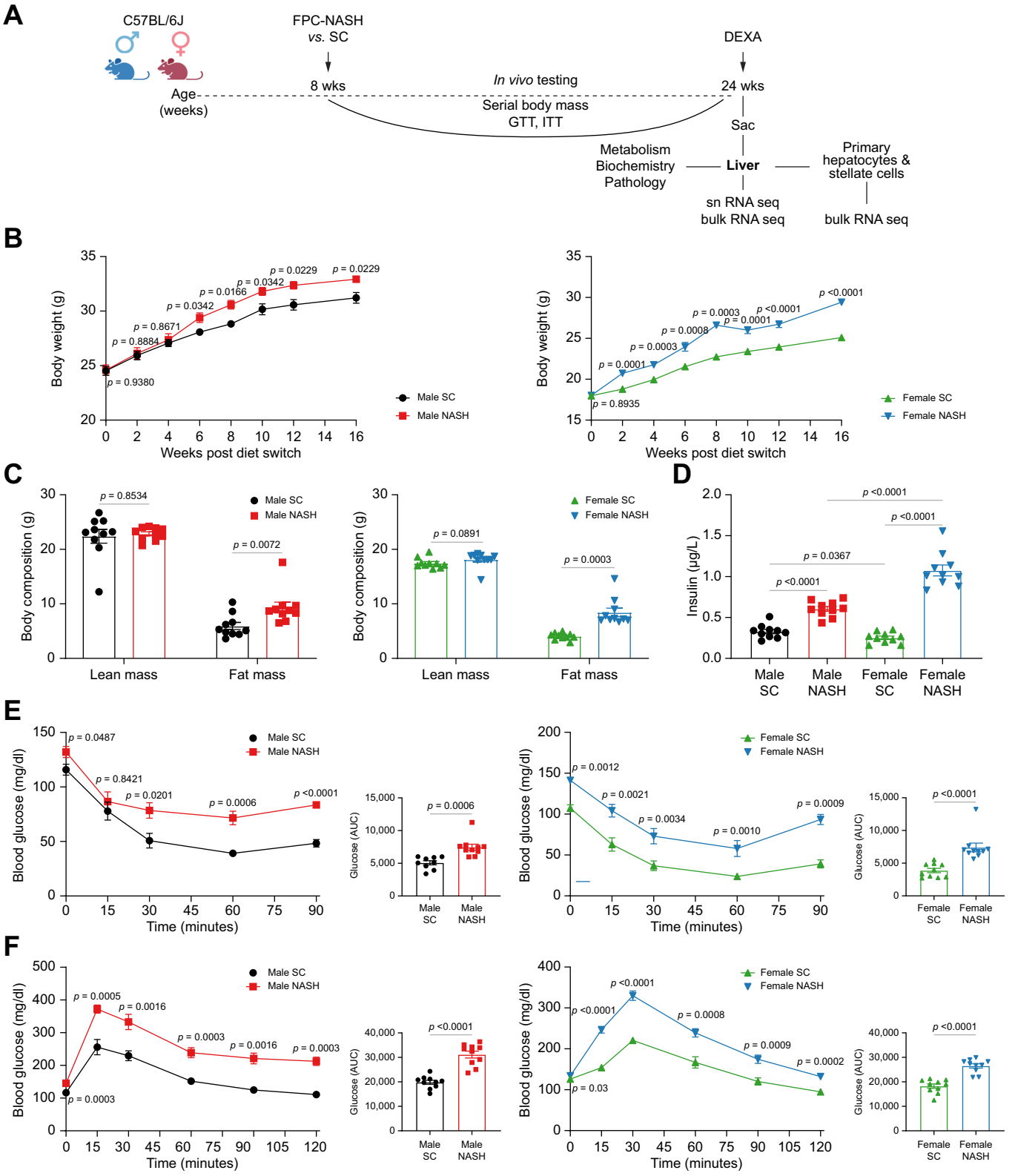

Fig. 1. FPC-NASH diet increases body mass and adiposity and perturbs insulin and glucose tolerance in male and female mice. (A) Experimental schematic (Created with BioRender.com). For B,C,D,E,F, unpaired t test for group comparisons at each time point was employed. For group comparison, the Shapiro–Wilk normality test was conducted first for each group with prespecified significance level of 0.05, and if passed, the t test was implemented whereas the non-parametric Wilcoxon rank-sum test was used if normality was not established. False discovery rate-adjusted *p* values are reported in multiple hypothesis testing. (B) Body mass recorded over the indicated time course in male and female mice fed SC or FPC-NASH from 8 weeks of age for 16 weeks (n = 10 mice/group). At 16 weeks diet, Male NASH *vs.* Male SC, $p = 0.0229$ and Female NASH *vs.* Female SC, $p < 0.0001$. (C) Lean mass and fat mass measured by DEXA in male and female mice after 16 weeks of diet. Male mice: Lean mass: Male

in contrast, no significant association was noted between the consumption of diet soda and fatty liver disease. Stanhope and colleagues compared the effects of the addition of isocaloric glucose- and fructose-sweetened beverages to diet in adults with overweight or obesity. Although both interventions increased body mass, the addition of fructose, not glucose, caused increased visceral adiposity, hepatic *de novo* lipogenesis, dyslipidemia, and insulin resistance.[13] A subsequent study reported that the combined intake of fructose and glucose was likely more harmful than fructose alone.[14]

Because of the sequelae of MASLD/MASH,[2] numerous animal models have been developed to probe mechanisms and therapeutic opportunities in MASH. They range from methionine/choline-deficient diets, in which mice may lose weight over the course of feeding, to diets that replicate some of the body mass and metabolic perturbations that have been associated with MASLD/MASH, such as the addition of high-fat and cholesterol.[15,16] A recent study suggested that dietary enrichment of fat and fructose in mice resulted in pathology that resembled human MASLD.[16] The addition of high-fat and cholesterol to a fructose-containing diet aimed to recapitulate facets of the "Western diet".[17] Despite the importance of MASLD/MASH in both men and women, only 5% of preclinical studies were reported to include both male and female mice.[16]

We sought to address the effects of dietary fat and fructose on both male and female C57BL/6J mice fed a fructose, palmitate and cholesterol ("FPC") "non-alcoholic steatohepatitis" (NASH) diet *vs.* standard chow (SC).[17] Surprisingly, although both male and female mice developed increased body mass, adiposity, and insulin and glucose intolerance after 16 weeks of FPC-NASH diet, female mice displayed greater hepatic triglyceride content, inflammation, fibrosis and MASH score. To address the molecular basis of these observed sex differences, we performed single-nucleus RNA sequencing (snRNAseq) of the liver and validated findings through bulk RNAseq of whole liver and of isolated primary hepatocytes and stellate cells. We analyzed differentially expressed genes (DEGs), pathways, transcriptional regulation networks and the metabolic fluxome in mouse and human livers, the latter through the examination of publicly available data sets of male and female patients with MASH.

Materials and methods

See supplementary information for detailed materials and methods.

Results

FPC-NASH diet increases body mass and adiposity and perturbs insulin and glucose tolerance in male and female mice

Male and female C57BL/6J mice were randomly assigned to an FPC-NASH diet[17] or SC for 16 weeks, beginning at age 8 weeks (Fig. 1A). After 16 weeks, male and female mice fed an FPC-NASH diet (hereafter referred to as FPC-NASH) displayed significantly higher body mass *vs.* mice fed SC ($p = 0.0229$ and $p < 0.0001$, respectively; Fig. 1B). By dual-energy x-ray absorptiometry scanning, after 16 weeks, male and female mice fed FPC-NASH displayed increased fat mass *vs.* mice fed SC ($p = 0.0072$ and $p = 0.0003$, respectively; Fig. 1C). There were no significant within-sex differences in lean mass between mice fed FPC-NASH *vs.* SC (Fig. 1C). Plasma concentrations of insulin were higher in male and female mice fed FPC-NASH *vs.* SC ($p < 0.0001$) and were significantly higher in FPC-NASH-fed female *vs.* male mice ($p < 0.0001$; Fig. 1D). Male and female mice fed FPC-NASH *vs.* SC demonstrated significantly impaired insulin tolerance by area under the curve ($p = 0.0006$ and $p < 0.0001$, respectively; Fig. 1E) and by percent change in concentrations of glucose compared to baseline ($p = 0.0029$ and $p = 0.0051$, respectively; Fig. S1A,B). Similarly, glucose tolerance was impaired in both male and female mice fed FPC-NASH *vs.* SC, as assessed by area under the curve ($p < 0.0001$; Fig. 1F) and by the percent change from baseline ($p = 0.0036$ and $p < 0.0001$, respectively; Fig. S1C,D). Taken together, both male and female mice developed increased body mass and adiposity, and insulin and glucose intolerance, when fed FPC-NASH *vs.* SC for 16 weeks.

FPC-NASH causes sex-dependent abnormalities in plasma and hepatic lipid content

To test the effects of FPC-NASH *vs.* SC on hepatic dysfunction and MASLD/MASH, we assayed the plasma concentrations of two liver enzymes, ALT and aspartate aminotransferase (AST). In male not female mice fed FPC-NASH *vs.* SC, plasma concentrations of AST were higher ($p = 0.0002$ and $p = 0.1899$, respectively). Plasma concentrations of ALT were higher in male and female mice fed FPC-NASH *vs.* SC ($p = 0.0025$ and $p = 0.0020$, respectively; Fig. 2A,B). There were no significant differences in plasma concentrations of AST or ALT when comparing male *vs.* female mice fed FPC-NASH ($p = 0.0528$ and $p = 0.6112$, respectively; Fig. 2A,B).

Plasma concentrations of cholesterol were significantly higher in male and female mice fed FPC-NASH *vs.* SC ($p = 0.0003$) and were significantly higher in female *vs.* male mice fed FPC-NASH ($p = 0.0102$; Fig. 2C). Similarly, both male and female mice fed FPC-NASH developed significantly higher plasma concentrations of triglycerides *vs.* SC-fed mice ($p < 0.0001$), which were significantly higher in female *vs.* male mice fed FPC-NASH ($p < 0.0001$; Fig. 2D).

We performed Oil Red O staining of the livers to detect neutral lipids (Fig. S2A). Quantification revealed significantly higher Oil Red O-positive area in male and female mice fed an FPC-NASH diet *vs.* SC ($p = 0.0389$ and $p = 0.0011$, respectively). There were no significant differences in Oil Red O staining in female *vs.* male mice fed FPC-NASH ($p = 0.0626$; Fig. 2E). The hepatic triglyceride content was significantly

NASH *vs.* Male SC, $p = 0.8534$ and Fat mass: Male NASH *vs.* Male SC, $p = 0.0072$. Female mice: Lean mass: Female NASH *vs.* Female SC, $p = 0.0891$ and Fat mass: Female NASH *vs.* Female SC, $p = 0.0003$. (D) Post-6-hour fast measurement of plasma concentrations of insulin in male and female mice after 16 weeks of diet. Male NASH *vs.* Male SC, $p < 0.0001$; Female NASH *vs.* Female SC, $p < 0.0001$; Female SC *vs.* Male SC, $p = 0.0367$ and Female NASH *vs.* Male NASH, $p < 0.0001$. (E) Post-6-hour fast insulin tolerance test in male and female mice after 14 weeks of diet. AUC: Male NASH *vs.* Male SC, $p = 0.0006$ and Female NASH *vs.* Female SC, $p < 0.0001$. (F) Post-6-hour fasting glucose tolerance test in male and female mice after 15 weeks of diet. AUC: Male NASH *vs.* Male SC, $p < 0.0001$ and Female NASH *vs.* Female SC, $p < 0.0001$. Data are presented as the mean ± SEM. Multiple cohorts were employed for replication and to execute all the biochemical, molecular, and physiological studies reported in this figure. AUC, area under the curve; DEXA, dual-energy x-ray absorptiometry; GTT, glucose tolerance test; ITT, insulin tolerance test.

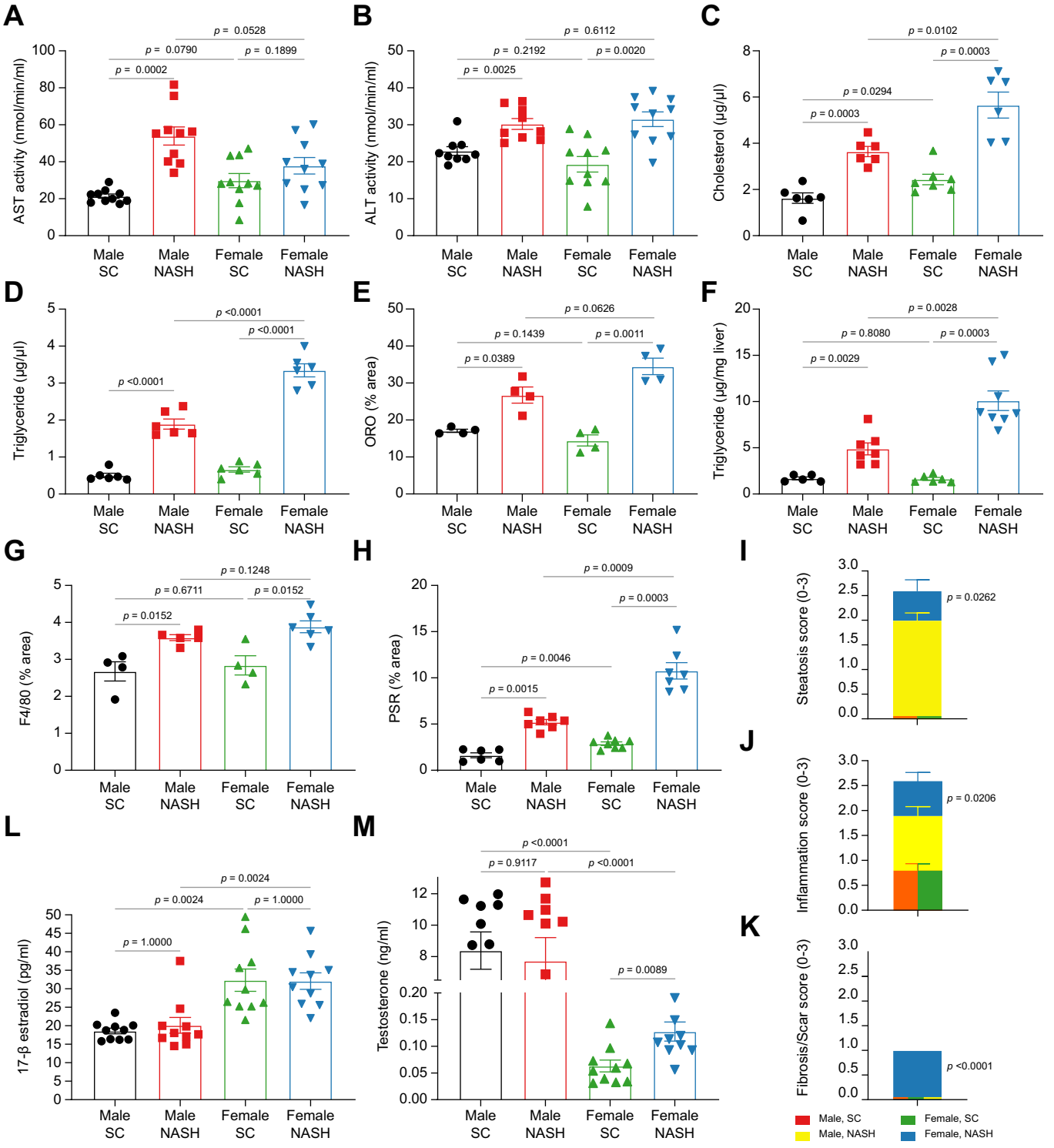

Fig. 2. Effect of sex on lipid metabolism and pathology in response to FPC-NASH *vs.* SC. (A-H) For group comparison, the Shapiro–Wilk normality test was conducted first for each group with prespecified significance level of 0.05, and if passed, the t test was implemented whereas the non-parametric Wilcoxon rank-sum test was used if normality was not established. False discovery rate-adjusted *p* values are reported in multiple hypothesis testing. (A-B) Liver AST and ALT activity assay, respectively, measured in male and female mice after 14 weeks of diet. AST: Male NASH *vs.* Male SC, $p = 0.0002$; Female NASH *vs.* Female SC, $p = 0.1899$; Female SC *vs.* Male SC, $p = 0.0790$; and Female NASH *vs.* Male NASH, $p = 0.0528$. ALT: Male NASH *vs.* Male SC, $p = 0.0025$; Female NASH *vs.* Female SC, $p = 0.0020$; Female SC *vs.* Male SC, $p = 0.2192$; and Female NASH *vs.* Male NASH, $p = 0.6112$. (C-D) Randomly fed plasma cholesterol and triglyceride concentrations were measured after 16 weeks of diet. Cholesterol: Male NASH *vs.* Male SC, $p = 0.0003$; Female NASH *vs.* Female SC, $p = 0.0003$; Female SC *vs.* Male SC, $p = 0.0294$; and Female NASH *vs.* Male NASH, $p = 0.0102$. Triglyceride: Male NASH *vs.* Male SC, $p < 0.0001$; Female NASH *vs.* Female SC, $p < 0.0001$; and Female NASH *vs.* Male NASH $p < 0.0001$. (E) Oil Red O staining of the liver quantified as positive area (%) (n = 6 per group with 5-6 images per sample) in male and female mice after 16 weeks of diet. Male NASH *vs.* Male SC, $p = 0.0389$; Female NASH *vs.* Female SC, $p = 0.0011$; Female SC *vs.* Male SC, $p = 0.1439$; and Female NASH *vs.* Male NASH, $p = 0.0626$. (F) Liver triglyceride content after 16 weeks of diet. Male NASH *vs.* Male SC, $p = 0.0029$; Female NASH *vs.* Female SC, $p = 0.0003$; Female SC *vs.* Male SC, $p =$

higher in female and male mice fed FPC-NASH *vs.* SC (p = 0.0029 and p = 0.0003, respectively), and in female *vs.* male mice fed FPC-NASH (p = 0.0028; Fig. 2F). Thus, female mice develop greater steatosis than male mice fed FPC-NASH.

Exacerbation of inflammation, steatosis and fibrosis in female *vs.* male mice fed FPC-NASH

To assess the livers for inflammation, we performed immunohistochemistry for macrophage marker F4/80 antigen (Fig. S2B). As shown in Fig. 2G, both male and female mice fed FPC-NASH *vs.* SC developed a greater F4/80-positive area (p = 0.0152). There were no differences between FPC-NASH-fed female *vs.* male mice (p = 0.1248). We performed picrosirius red staining to detect fibrosis (Fig. S2A). Quantification revealed that the picrosirius red-positive area was significantly greater in male and female mice fed FPC-NASH *vs.* SC (p = 0.0015 and p = 0.0003, respectively). The picrosirius red-positive area was significantly greater in female *vs.* male mice fed FPC-NASH (p = 0.0009; Fig. 2H).

We performed MASH scoring based on published criteria and assessment of steatosis (0-3), inflammation (0-3) and fibrosis/scar (0-3).[18] Significantly higher steatosis scores were observed in female FPC-NASH *vs.* male FPC-NASH-fed mice (p = 0.0262; Fig. 2I). Significantly higher inflammation scores were observed in female FPC-NASH- *vs.* male FPC-NASH-fed mice (p = 0.0206; Fig. 2J). Significantly higher fibrosis scores were observed in female FPC-NASH- *vs.* male FPC-NASH-fed mice; p <0.0001 (Fig. 2K). In summary, female mice develop greater hepatic steatosis, inflammation and fibrosis than male mice fed the FPC-NASH diet.

To investigate potential mechanisms underlying these sex-dependent effects, we analyzed plasma sex hormone concentrations. After synchronizing the female mice's hormonal cycle, we measured plasma concentrations of 17-beta-estradiol. 17-beta-estradiol levels showed no significant differences between FPC-NASH and SC diets within each sex (Fig. 2L). Next, we measured plasma concentrations of testosterone. Testosterone analysis revealed higher overall concentrations in males, as expected. Interestingly, while male mice showed no difference in testosterone levels between diets (p = 0.9117), female mice fed FPC-NASH exhibited significantly higher testosterone levels compared to those on SC (p = 0.0089) (Fig. 2M). This diet-induced change in testosterone levels in females but not in males suggests a potential role for altered hormone balance in the exacerbated liver pathology observed in females.

FPC-NASH diet alters plasma concentrations of adiponectin and leptin in mice

As significant perturbations of metabolism, body mass and adiposity due to FPC-NASH were observed, we tested the effects of FPC-NASH on plasma concentrations of adiponectin and leptin in female and male mice. In male mice, no diet-dependent differences in plasma concentrations of adiponectin were observed; in female mice, animals fed FPC-NASH *vs.* SC displayed significantly lower plasma concentrations of adiponectin (p <0.0001; Fig. S2C). Female mice fed FPC-NASH demonstrated significantly lower plasma concentrations of adiponectin *vs.* male mice (p = 0.0002; Fig. S2C). Both male and female mice fed FPC-NASH displayed significantly higher plasma concentrations of leptin *vs.* male and female mice fed SC (p = 0.0027 and p <0.0001, respectively; Fig. S2D). Plasma concentrations of leptin were significantly higher in female *vs.* male mice fed FPC-NASH (p = 0.0005; Fig. S2D). We calculated the adiponectin/leptin ratio, a marker of adipose tissue dysfunction.[19,20] In both male and female mice, when comparing FPC-NASH *vs.* SC, significantly lower adiponectin/leptin ratios were noted (p = 0.0044 and p = 0.0019, respectively; Fig. S2E). The adiponectin/leptin ratio was significantly lower in female *vs.* male mice fed FPC-NASH (p = 0.0002; Fig. S2E).

Taken together, both male and female mice fed FPC-NASH over 16 weeks developed increased body mass and adiposity and perturbations in glucose and insulin tolerance. Female mice developed more severe hepatic steatosis and fibrosis *vs.* male mice fed FPC-NASH. To dissect the underlying mechanisms, we performed snRNAseq of liver tissue from male and female mice fed FPC-NASH or SC. Validation experiments of

0.8080; and Female NASH *vs.* Male NASH, p = 0.0028. (G) F4/80 staining of the liver quantified as positive area (%) (5-6 images per unique sample) in male and female mice after 16 weeks of diet. Male NASH *vs.* Male SC, p = 0.0152; Female NASH *vs.* Female SC, p = 0.0152; Female SC *vs.* Male SC, p = 0.6711; and Female NASH *vs.* Male NASH, p = 0.1248. (H) Picrosirius red staining of the liver quantified as positive area (%) (5-6 images per unique sample) in male and female mice after 16 weeks of diet. Male NASH *vs.* Male SC, p = 0.0015; Female NASH *vs.* Female SC, p = 0.0003; Female SC *vs.* Male SC, p = 0.0046; and Female NASH *vs.* Male NASH, p = 0.0009. (I–K) After 16 weeks FPC-NASH *vs.* SC diet, livers were removed and subjected to special stains (H&E and picrosirius red) for the detection and scoring of (I) steatosis; (J) inflammation; and (K) fibrosis/scar. In 10 mice per sex per diet, the following scores were assigned by a co-author (NDT) naïve to the experimental condition. Mean score per criterion ± SEM and statistical analyses are as follows: In (I- Steatosis), Male SC, 0 ± 0; Male NASH, 2 ± 0.1491; Female SC, 0 ± 0; and Female NASH, 2.6 ± 0.2211. Statistical analyses were performed using the Wilcoxon rank-sum test: Male SC *vs.* Male NASH, p <0.0001; Female SC *vs.* Female NASH, p <0.0001; and Female NASH *vs.* Male NASH, p = 0.0262. In (J-Inflammation), Male SC, 0.8 ± 0.1333; Male NASH, 1.9 ± 0.1795; Female SC, 0.8 ± 0.1333; and Female NASH, 2.6 ± 0.1633. Statistical analyses were performed using the Wilcoxon rank-sum test: Male SC *vs.* Male NASH, p = 0.0012; Female SC *vs.* Female NASH, p = 0.0003; and Female NASH *vs.* Male NASH, p = 0.0206. In (K-Fibrosis/scar), Male SC, 0 ± 0; Male NASH, 0 ± 0; Female SC, 0 ± 0; and Female NASH, 1.0 ± 0. Statistical analyses were performed using the Wilcoxon rank-sum test: Female SC *vs.* Female NASH, p <0.0001; and Female NASH *vs.* Male NASH, p <0.0001. Multiple cohorts were employed for replication and to execute all the biochemical, molecular, and physiological studies reported in this figure. For (A-H) for group comparison, the Shapiro–Wilk normality test was conducted first for each group with prespecified significance level of 0.05, and if passed, the t test was implemented whereas the non-parametric Wilcoxon rank-sum test was used if normality was not established. False discovery rate-adjusted p values are reported in multiple hypothesis testing. (L-M). Plasma concentrations of sex hormones. Plasma 17-beta-estradiol (L) and testosterone (M) concentrations were measured after 16 weeks of diet in 10 mice per sex per diet. Statistical analyses for L-M, 17-beta estradiol and for testosterone concentrations were performed using the Wilcoxon rank-sum test. Multiple cohorts were employed for replication and to execute the biochemical studies reported in this figure. For group comparison, the Shapiro–Wilk normality test was conducted first for each group with prespecified significance level of 0.05, and if passed, the t test was implemented whereas the non-parametric Wilcoxon rank-sum test was used if normality was not established. False discovery rate-adjusted p values are reported in multiple hypothesis testing. 17-beta estradiol: Male NASH *vs.* Male SC, p = 1.0000; Female NASH *vs.* Female SC, p = 1.0000; Female SC *vs.* Male SC, p = 0.0024; and Female NASH *vs.* Male NASH, p = 0.0024. Testosterone: Male NASH *vs.* Male SC, p = 0.9117; Female NASH *vs.* Female SC, p = 0.0089; Female SC *vs.* Male SC, p <0.0001.; and Female NASH *vs.* Male NASH, p <0.0001. ALT, alanine aminotransferase; AST, aspartate aminotransferase; ORO, oil red O; PSR, Picrosirius Red.

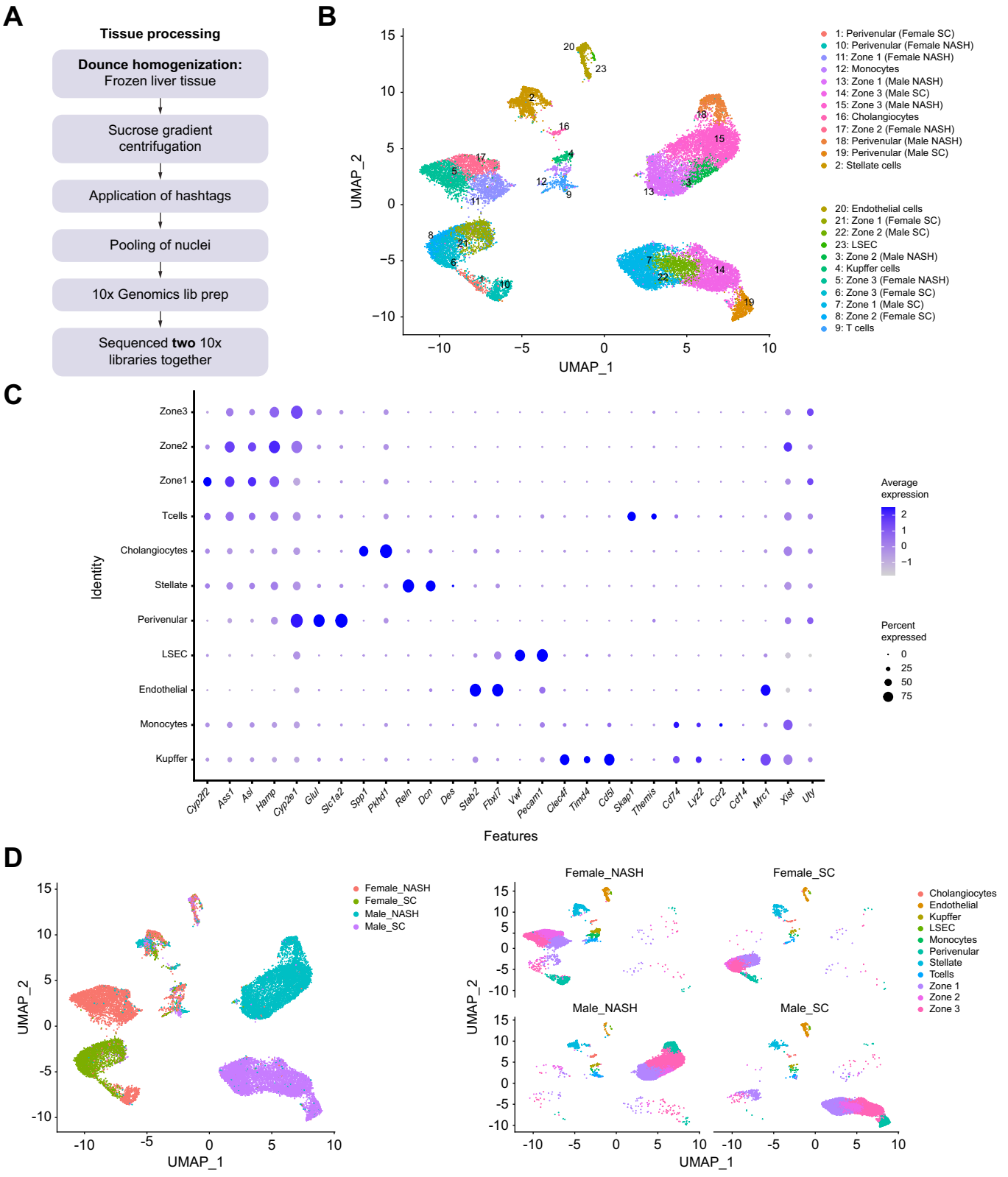

Fig. 3. Single-nucleus RNAseq: Quality control and identification of cellular clusters. (A) Preparation and hash-tagging of nuclei for single-nucleus RNAseq in four distinct experimental groups of mice: Female mice, FPC-NASH ("NASH"); Female mice, standard chow (SC); Male mice, NASH; and Male mice, SC. (B) UMAP visualization of all nuclei, showing clusters found using SNN modularity optimization-based clustering algorithm in Seurat. Clusters were manually annotated using known marker genes. (C) Dot plot showing expression of known marker genes and the proportion of cells that express the marker genes across all cell types (D) (Left) UMAP visualization showing nuclei colored by condition (sex and diet combination); (Right) UMAP visualization showing nuclei colored by cell type, split by condition. SNN, shared nearest neighbor; UMAP, Uniform Manifold Approximation and Projection.

bulk RNAseq on whole liver or isolated primary hepatocytes and stellate cells from the four groups of mice (both sexes/both diets) were also performed.

SnRNAseq: Quality controls and identification of cellular clusters

At the conclusion of 16 weeks FPC-NASH *vs.* SC, livers were extracted from male and female mice and subjected to snRNAseq; samples were hash-tagged with unique nuclear antibodies in duplicate (Fig. 3A). Demultiplexing and quality control (QC) were performed for each batch.[21] The uniform manifold approximation and projection (UMAP) for dimension reduction was used and UMAPs are shown in Fig. S3A,B. In both batches, filtering was performed based on the number of expressed genes, number of reads, percent reads derived from mitochondrial genes, presence of ambient RNA and the presence of doublets. Batch 1 contained 10,176 nuclei and Batch 2 contained 12,366 nuclei. After QC and preprocessing, we integrated the batches and visualized the structure of the integrated data in a UMAP plot (Fig. S3C). Fig. 3B shows all cells in the dataset colored by the 23 clusters identified in Seurat. These clusters were assigned to 11 cell types, including hepatocytes (zones 1, 2, and 3 and perivenular hepatocytes); cholangiocytes; endothelial cells; liver sinusoidal endothelial cells (LSECs); stellate cells; monocytes; Kupffer cells; and T cells, which were identified based on published marker genes. Table S1 lists all cluster markers found in Seurat and the dot plot in Fig. 3C illustrates gene markers by cluster name. Note that the largest clusters contain hepatocytes, which can be subdivided into hepatocytes in zones 1, 2, and 3 and perivenular hepatocytes. The hepatocytes clearly separate by sex and diet, indicating that both sex and diet have strong influences on the hepatocyte transcriptome (Fig. 3D). To validate the identity of zonal and perivenular hepatocytes, we conducted spatial transcriptomics analysis on liver tissue from two male mice fed FPC-NASH for 16 weeks (Fig. S3D,E). Based on published literature,[22] marker genes used to identify hepatocyte subtypes are expressed in distinct areas of the liver in spatial transcriptomics data of two different mouse liver samples: Zone 1, *Cyp2f2*; Zone 2, *Ass1* and *Asl*; Zone 3, *Cyp2e1*; and perivenular hepatocytes, *Glul* and *Slc1a2*. This spatial analysis corroborated our cluster assignments.

SnRNAseq: characterizing differences in hepatocyte proportions and transcriptional profiles

We investigated the effects of sex and diet on the hepatocyte clusters. Fig. 4A illustrates the UMAP plot for hepatocytes in zones 1, 2, and 3 and perivenular hepatocytes and Fig. 4B reveals significant differences by sex (*Xist*, female and *Uty*, male) and the liver zonation (*Cyp2f2*, Zone 1; *Asl*, Zone 2; *Cyp2e1*, Zone 3; and *Glul*, perivenular hepatocytes). We examined the proportion of cell types between the conditions and found differences between female and male FPC-NASH as follows: females fed FPC-NASH tend to have a larger proportion of zone 2 hepatocytes *vs.* males on FPC-NASH. No significant differences were observed among any of the hepatocyte cell types in female *vs.* male mice fed SC after correction for multiple testing (Fig. 4C). Table S1 details the comprehensive differential cell type abundance analysis and the number of cells per group per batch.

To investigate how female *vs.* male mice responded to the FPC-NASH diet, we performed pseudobulk differential expression analysis using DESeq2 (q-value of 0.1). Fig. 4D reveals that the cell types that respond most strongly to FPC-NASH and that display the largest differences in transcriptional profiles between female and male mice are hepatocytes and stellate cells. These data reveal that within-sex, female and male mice differ in their transcriptional profiles during SC feeding and that differences are amplified by FPC-NASH. Based on the observation that hepatocyte zones 1, 2, and 3 have a similar transcriptional response, we displayed these data as "merged" DEGs among zones 1, 2, and 3 (Fig. 4E). Analysis of gene ontology (GO) terms among zones 1, 2, and 3 and perivenular hepatocytes reveals that zones 1, 2 and 3 are more similar and that they display a different pattern of GO terminologies displayed by the perivenular hepatocytes (Fig. 4F). Therefore, we further examined "merged hepatocytes 1, 2 and 3" and, separately, perivenular hepatocytes.

SnRNAseq: Effect of sex and diet on hepatocyte gene expression

We examined the hepatocyte-related DEGs in more detail by visualizing their expression patterns in all treatments and conditions. The heatmap in Fig. 4G displays the expression of all DEGs across the four conditions (red, higher expression and blue, lower expression, with each row representing a gene). The heatmap displays the division of genes into nine groups by applying a hierarchical cluster algorithm to the gene expression values across the four experimental groups. Summary line plots of all nine groups shown in Fig. S4A reveal the average response of the genes in each group. Bar plots illustrate the GO terms that display a sex-by-diet interaction response (Groups 1, 2, 4, 7, and 8) (Fig. 4H); a sex-specific response (Group 6) (Fig. 4I) or a diet-specific response (Groups 3 and 5) (Fig. 4J). No significant functional enrichment was found for group 9. GO terms indicative of fatty acid metabolism, mitochondrial organization and function and general metabolic pathways displayed significant sex-by-diet interaction response differences between female and male mice on FPC-NASH. Analogous findings were identified when the hepatocyte zones 1, 2, and 3 were considered individually (Figs S5-7).

In addition to hepatocyte zones 1, 2, and 3, we also analyzed the perivenular hepatocytes. We display the expression of all DEGs across the four conditions and based on the patterns shown in the heatmap, divided the genes into six groups (Fig. S4B); the summary line plots are shown in Fig. S4C. Four of the groups displayed significant sex-by-diet interaction responses (Fig. S4D) and two of the groups displayed sex-specific responses (Fig. S4E). Of those displaying significant sex-by-diet interaction responses, GO terms were related to lipid and cholesterol metabolism, mitochondrial metabolism and cellular signaling, which were generally similar to the pathways identified in the merged zones 1, 2, and 3 hepatocytes.

To elucidate sex-specific responses to the FPC-NASH diet, we conducted differential gene expression analysis on merged hepatocyte zones 1, 2, and 3, comparing FPC-NASH to SC within each sex. The plot shown in Fig. S8A illustrates that there were 118 and 148 uniquely downregulated DEGs in male FPC-NASH *vs.* SC and female FPC-NASH *vs.* SC-fed mice,

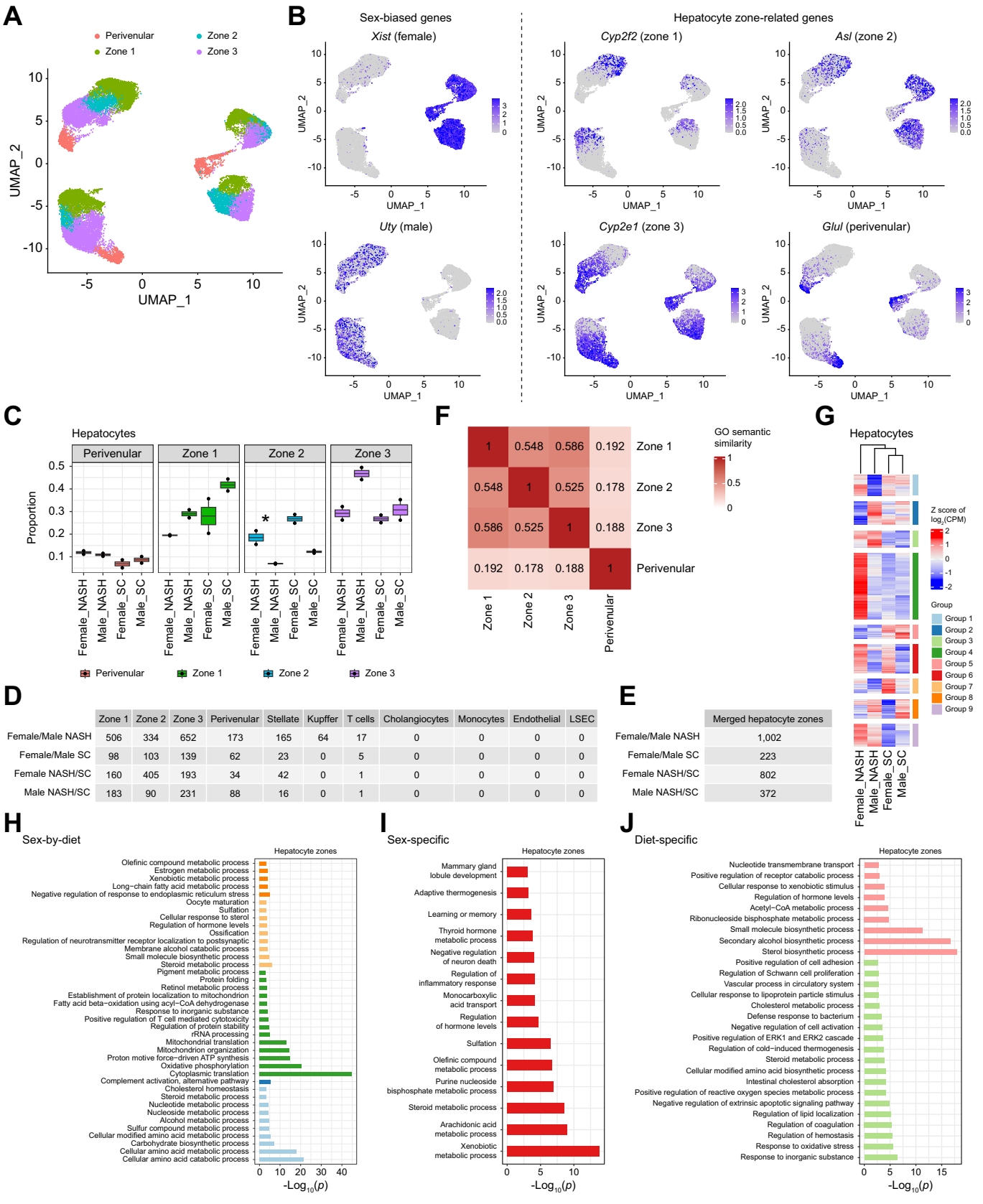

	Zone 1	Zone 2	Zone 3	Perivenular	Stellate	Kupffer	T cells	Cholangiocytes	Monocytes	Endothelial	LSEC
Female/Male NASH	506	334	652	173	165	64	17	0	0	0	0
Female/Male SC	98	103	139	62	23	0	5	0	0	0	0
Female NASH/SC	160	405	193	34	42	0	1	0	0	0	0
Male NASH/SC	183	90	231	88	16	0	1	0	0	0	0

	Merged hepatocyte zones
Female/Male NASH	1,002
Female/Male SC	223
Female NASH/SC	802
Male NASH/SC	372

Fig. 4. Single-nucleus RNAseq: Hepatocytes and DEGs using pseudobulk differential expression analysis. (A) UMAP visualization of hepatocyte nuclei, colored by hepatocyte zones 1, 2, and 3 and the perivenular hepatocytes. (B) (Left) Cell-based expression patterns of sex-specific genes and (Right) illustration of zone-specific genes for hepatocytes (zones 1, 2, and 3 and perivenular); (C) Proportions of hepatocyte subtypes across conditions. *Indicates a significantly larger proportion of zone 2 hepatocytes in female *vs.* male FPC-NASH (propeller differential proportion test q-value = 0.038). (D) Number of DEGs identified for the indicated pairwise contrasts

respectively. There were 118 and 518 differentially expressed upregulated genes in male FPC-NASH *vs.* SC and female FPC-NASH *vs.* SC-fed mice, respectively (Fig. S8A). Common to both sexes, there were 55 downregulated DEGs in male FPC-NASH *vs.* SC and female FPC-NASH *vs.* SC-fed mice, and 77 common upregulated DEGs in male FPC-NASH *vs.* SC and female FPC-NASH *vs.* SC-fed mice. Finally, there were four downregulated DEGs in male FPC-NASH *vs.* male SC that were upregulated DEGs in female FPC-NASH *vs.* female SC-fed mice (Fig. S8A) (Table S1).

Next, we sought to identify the pathways represented by these within-sex diet-dependent DEGs. With respect to genes downregulated in either male or female FPC-NASH *vs.* SC, in both sexes, the chief pathways that were downregulated related to metabolism; however, the overall number of pathways affected in males was greater than that in females (Fig. S8B). In males, downregulated pathways in FPC-NASH *vs.* SC related to metabolism of steroids, organic hydroxy compounds, xenobiotics, ribonucleosides, sterols, sulfur, energy reserve, and amino acids. In females, steroid metabolic pathways were downregulated; however, unique to females, regulation of hormone levels was downregulated, suggesting a potential basis for sex differences. Pathways downregulated in FPC-NASH *vs.* SC in both sexes were related to metabolism (sterol, secondary alcohol, dicarboxylic, ribose, purine and xenobiotic), and negative regulation of collagen biosynthesis in FPC-NASH *vs.* SC was identified in both sexes, suggesting impact on tissue scarring mechanisms (Fig. S8B).

In the case of upregulated genes in either male or female mice fed FPC-NASH *vs.* SC, pathways related to thrombosis/hemostasis, wound healing and xenobiotic transport were identified in males (Fig. S8B), while pathways related to mitochondrial translation and organization and metabolism (ATP, phenylpropanoid, steroid, xenobiotic, olefinic compound, organic hydroxy compound and pigment) were identified in females (Fig. S8B). Upregulated pathways common to both sexes included those related to inflammation, intestinal cholesterol absorption and cholesterol transport, as well as lipid catabolism and hyaluron metabolism (Fig. S8B).

Collectively, these data suggest that multiple metabolic processes tended to be downregulated in male FPC-NASH *vs.* SC, whereas many more metabolic processes, and particularly those related to mitochondrial function and metabolism, were upregulated in the females. Further, female not male hepatocytes demonstrated downregulation of pathways related to hormone levels and male not female hepatocytes displayed upregulation of pathways related to wound healing and thrombosis/hemostasis, such as markers of fibrinolysis, which suggest enhanced tissue remodeling and reduced potential for scarring in male *vs.* female hepatocytes in FPC-NASH *vs.* SC (Fig. S8B).

We then aimed to validate our snRNAseq findings. First, we performed bulk RNAseq on whole livers of male and female mice fed FPC-NASH or SC. Deconvolution of bulk RNAseq revealed that the cell types expressing the greatest enrichment of genes upregulated in female *vs.* male FPC-NASH-fed mice included stellate cells, endothelial cells, cholangiocytes, and Kupffer cells/monocytes (Fig. S9A). Hepatocyte deconvolution revealed a set of upregulated and downregulated genes in female *vs.* male FPC-NASH-fed mice (Fig. S9A) and GO term enrichment analysis revealed similar results to those observed in the merged hepatocyte zones and perivenular hepatocytes in the snRNAseq analysis, including processes related to lipid metabolism, mitochondrial function and general metabolic pathways (Fig. S9B). Downregulated terms enriched in female *vs.* male FPC-NASH hepatocytes were also related to metabolism (Fig. S9C). Table S2 contains details of the whole liver bulk RNAseq analysis.

A similar deconvolution analysis of the bulk RNAseq data performed in male and female mice fed SC revealed that cell types expressing the greatest enrichment of genes upregulated in female *vs.* male SC included endothelial cells, Kupffer cells/monocytes and T cells (Fig. S9D). Hepatocyte deconvolution revealed a set of upregulated and downregulated genes in female *vs.* male SC-fed mice (Fig. S9D). With respect to hepatocytes, enriched GO terms for genes upregulated in female *vs.* male SC-fed mice included ones related to cell migration, immune function and metabolism (Fig. S9E). Enriched GO terms for genes downregulated in female *vs.* male SC hepatocytes were similar to those for FPC-NASH (Fig. S9F).

We further performed bulk RNAseq on primary hepatocytes isolated from male and female mice fed FPC-NASH for 16 weeks. GO term enrichment analysis revealed up- and downregulation of processes that were very similar to those identified from snRNAseq and from deconvolution of bulk liver RNAseq data (Fig. S9G-H). Table S3 contains details of the bulk RNAseq analysis of isolated hepatocytes and stellate cells.

SnRNAseq: characterizing differences in non-hepatocyte proportions and transcriptional profiles

We investigated the effects of sex and diet on the non-hepatocyte clusters. Fig. 5A illustrates the UMAP plots representing the non-hepatocyte cell types (stellate cells, Kupffer cells, T cells, monocytes, cholangiocytes, endothelial cells and LSECs). We examined the proportion of cell types between the conditions and found that female mice fed FPC-NASH diet demonstrated a significantly larger proportion of endothelial cells and Kupffer cells and monocytes *vs.* male mice (Fig. 5B). These results support that female and male mice respond differently to the FPC-NASH diet. Table S1 details the comprehensive differential cell type abundance analysis.

With respect to DEGs, our analysis revealed 165, 23, 42, and 16 DEGs in stellate cells in female *vs.* male FPC-NASH-fed mice, in female *vs*. male SC-fed mice, in female FPC-NASH- *vs.* SC-fed mice, and in male FPC-NASH- *vs.* SC-fed mice, respectively (Fig. 4D). In contrast, the only other comparisons that revealed >5 DEGs in the non-hepatocyte clusters were the

for all cell types, based on pseudobulk differential expression analysis (q-value <0.1). (E) Number of DEGs identified for the indicated pairwise contrasts for merged hepatocyte zones based on pseudobulk differential expression analysis (q-value <0.1). (F) Semantic similarity analysis was used to assess similarity of significantly enriched GO terms across hepatocyte subtypes. (G) Normalized counts for all DEGs in merged hepatocyte zones, across the four conditions. DEGs were divided into nine groups using a hierarchical clustering algorithm. (H-J) Significantly enriched GO terms (Biological Process; q-value <0.05) for gene groups showing a (H) sex-by-diet interaction effect (Groups 1, 2, 4, 7, and 8); (I) sex-specific effect (Group 6); and (J) diet-specific effect (Groups 3 and 5). DEGs, differentially expressed genes; GO, Gene Ontology; UMAP, Uniform Manifold Approximation and Projection.

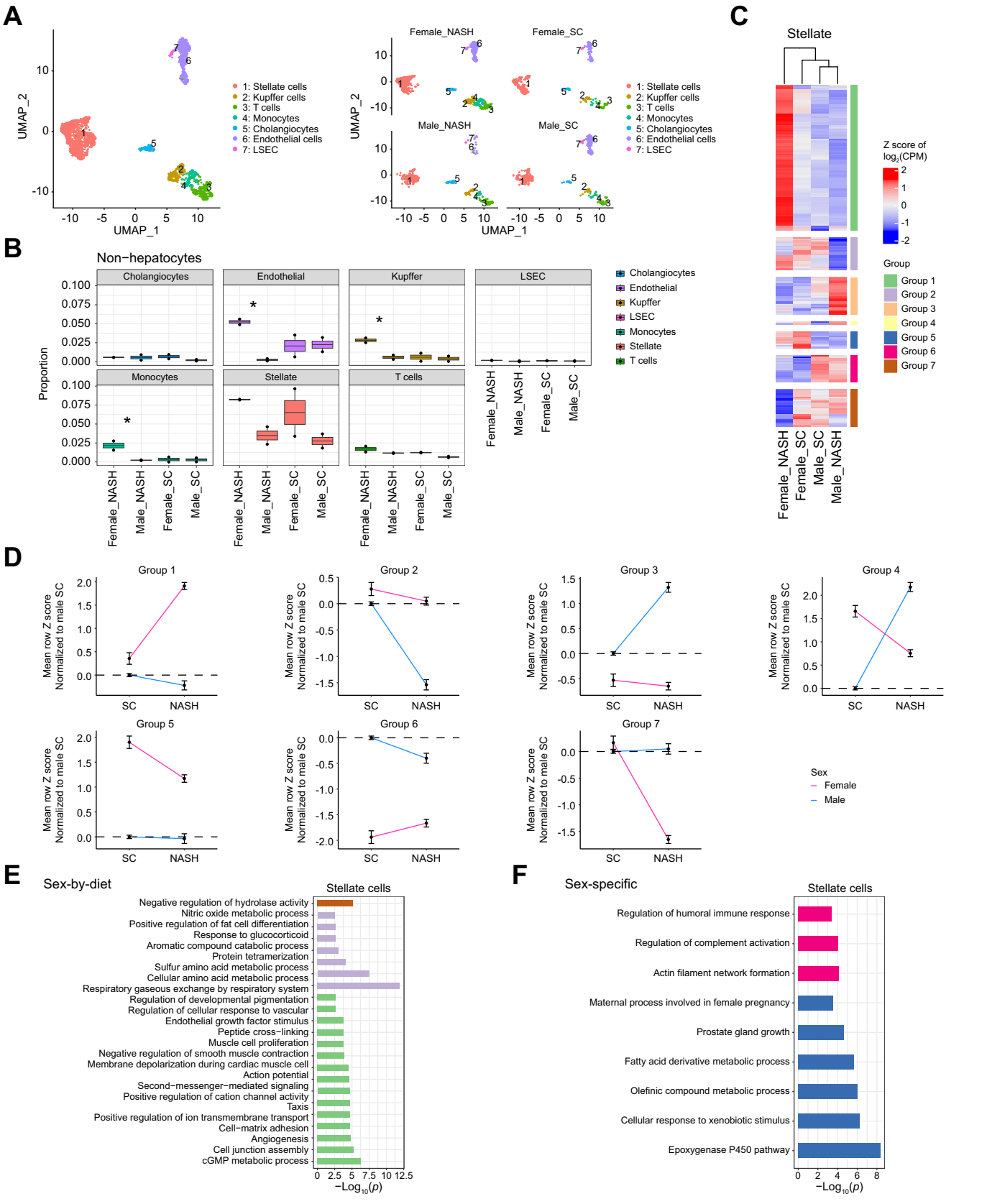

Fig. 5. Single-nucleus RNAseq: Effect of sex and diet on non-hepatocyte gene expression. (A) (Left) UMAP visualization of non-hepatocyte nuclei, colored by cell type; (Right) UMAP visualization showing non-hepatocyte nuclei colored by condition (sex and diet). (B) Proportions of non-hepatocyte cell types across conditions. *Indicates a significantly larger proportion of endothelial cells, Kupffer cells and monocytes in female *vs.* male FPC-NASH (propeller differential proportion test q-value for endothelial cells = 0.01; q-value for Kupffer cells = 0.038; q-value for monocytes = 0.01). (C) Normalized counts for all DEGs in stellate cells, across the four

Kupffer cells (64 DEGs in female *vs.* male mice fed FPC-NASH) and T cells (17 DEGs in female *vs*. male mice fed FPC-NASH) (Fig. 4D). Table S1 details the full list of DEGs in female *vs.* male mice and the enriched GO terms that significantly differed between the groups.

Based on these findings, we examined the DEGs in stellate cells by visualizing their expression patterns in all treatments and conditions. The heatmap in Fig. 5C displays the normalized and scaled expression of all DEGs across the four conditions (red, higher expression and blue, lower expression with each row representing a gene) in the stellate cell cluster. Based on these patterns, we divided the genes into seven groups. Summary line plots of all seven groups, shown in Fig. 5D, reveal the average response of the genes in each group and the GO terms that display a sex-by-diet interaction response (Groups 1, 2, and 7) (Fig. 5E) and a sex-specific response (Groups 5 and 6) (Fig. 5F). No significantly enriched terms were found for groups 3 and 4 (Fig. 5D). Nine GO terms indicative of amino acid metabolism, peptide cross-linking, cell-matrix adhesion and metabolic processes displayed significant sex-by-diet interaction differences in female *vs.* male FPC-NASH-fed mice. These data suggested that female *vs.* male FPC-NASH stellate cells were more metabolically active and amino acid metabolism suggests greater potential for extracellular matrix production.

Next, we performed additional analyses to characterize how stellate cells respond to the FPC-NASH *vs.* SC diet within each sex. Fig. S8C illustrates that there were 7 and 16 uniquely downregulated DEGs in male FPC-NASH- *vs.* SC- and female FPC-NASH *vs.* SC-fed mice, respectively. In the case of uniquely upregulated DEGs, there were 5 and 22 uniquely upregulated DEGs in male FPC-NASH- *vs.* SC- and female FPC-NASH *vs.* SC-fed mice, respectively (Fig. S8C). Common to both sexes, there were two downregulated DEGs in male FPC-NASH- *vs.* SC- and female FPC-NASH- *vs.* SC-fed mice, and two common upregulated DEGs in male FPC-NASH- *vs.* SC- and female FPC-NASH- *vs.* SC-fed mice.

We performed GO term enrichment analyses to identify the chief pathways represented by these within-sex and diet-dependent DEGs in stellate cells. In the case of downregulated unique genes in the male stellate cells, identified pathways were related to inflammation and to smooth muscle differentiation and distinct metabolic pathways (three) related to amino acid metabolism (Fig. S8D). In contrast, pathways related to uniquely downregulated genes in female FPC-NASH *vs.* SC stellate cells reflected nucelobase, nucleoside, deoxyribose phosphate, glycerolipid, and acetyl CoA metabolism (Fig. S8D). In the case of upregulated pathways in male FPC-NASH *vs.* SC, multiple pathways related to inflammation and those implicated in tissue reorganization such as response to wounding, angiogenesis, coagulation, hemostasis, epithelial cell proliferation, complement and plasminogen pathways were identified, suggesting an active extracellular matrix reorganization balanced with pathways to limit these processes. With respect to stellate cells in FPC-NASH- *vs.* SC-fed females, upregulated pathways were related to cell-cell adhesion, migration, chemotaxis and phosphatidylinositol 3-kinase signaling; there were pathways related to limitation of extracellular matrix expansion (Fig. S8D).

Pathways that were downregulated in both male and female stellate cells in FPC-NASH- *vs.* SC-fed mice were related to organic acid, tyrosine and triglyceride metabolism, as well as mitochondrial fission, DNA replication, response to glucocorticoid and thermogenesis and temperature regulation; whereas pathways upregulated in both male and female FPC-NASH- *vs.* SC-fed mice reflected cell adhesion molecules, mitosis and adherens junction organization (Fig. S8D).

Collectively, these data suggest that unlike female stellate cells, male stellate cells display unique upregulation of pathways related to inflammation and a balanced extracellular matrix reorganization, in which pathways such as coagulation, complement and plasminogen suggest limitation of extracellular matrix content. Downregulated pathways in male stellate cells reflected those related to amino acid metabolism (collagen production); in contrast, downregulation of these pathways was not noted in female stellate cells.

Next, to experimentally validate our findings in stellate cells, bulk RNAseq was performed on the whole livers of male and female mice fed either FPC-NASH or SC. With respect to the stellate cells, GO term analysis of the female *vs.* male enrichment in FPC-NASH revealed processes related to amino acid metabolism and fibroblast proliferation and organ growth (Fig. S10A). GO term analysis of the female *vs.* male enrichment in SC-fed mice revealed processes related to actin organization and immune cell activities (Fig. S10B). We also performed bulk RNAseq on isolated stellate cells from the female and male mice fed FPC-NASH. GO term enrichment analyses of the female *vs.* male FPC-NASH-fed mice revealed processes remarkably similar to those identified either from snRNAseq or deconvolution of bulk liver RNAseq data (Fig. S10C,D, respectively).

On account of the established roles of oxidative stress[23,24] and inflammation[25–27] in MASLD/MASH, we determined if these mechanisms were enriched in female *vs.* male mice in either FPC-NASH or SC conditions. We analyzed the genes identified through the GO terms “oxidative stress” and “inflammation” in merged or individual hepatocyte zones 1, 2, and 3; perivenular hepatocytes; and stellate cells. In Fig. S10E,F, in each cell type, lanes 1 and 2 reflect female *vs.* male FPC-NASH-fed mice and lanes 3 and 4 reflect SC-fed mice. First, the oxidative stress analysis is illustrated in Fig. S10E. The heat map reveals an upregulation of genes in females *vs.* males, particularly in FPC-NASH-fed mice, relevant to oxidative stress in hepatocyte zones 1, 2, and 3 (individual or merged), with overall much fewer differences in SC-fed mice. In the stellate cell cluster, most of these genes are not differentially expressed.

Similarly, we analyzed the genes related to the GO term “inflammation”. The heatmap in Fig. S10F shows that two sets of inflammation-related genes are found; one set that is predominantly expressed in hepatocytes and one set that is

conditions. DEGs were divided into seven groups using a hierarchical clustering algorithm. (D) Average expression per condition across genes in each group from Fig. 5C, normalized relative to male SC. Error bars show the standard error of the mean. (E) Significantly enriched GO terms (Biological Process; q-value <0.05) for gene groups showing a sex-by-diet interaction effect (Groups 1, 2, and 7). (F) Significantly enriched GO terms (biological process; q-value <0.05) for gene groups showing a sex-specific effect (Groups 5 and 6). GO, Gene Ontology; LSEC, liver sinusoidal endothelial cell; UMAP, Uniform Manifold Approximation and Projection

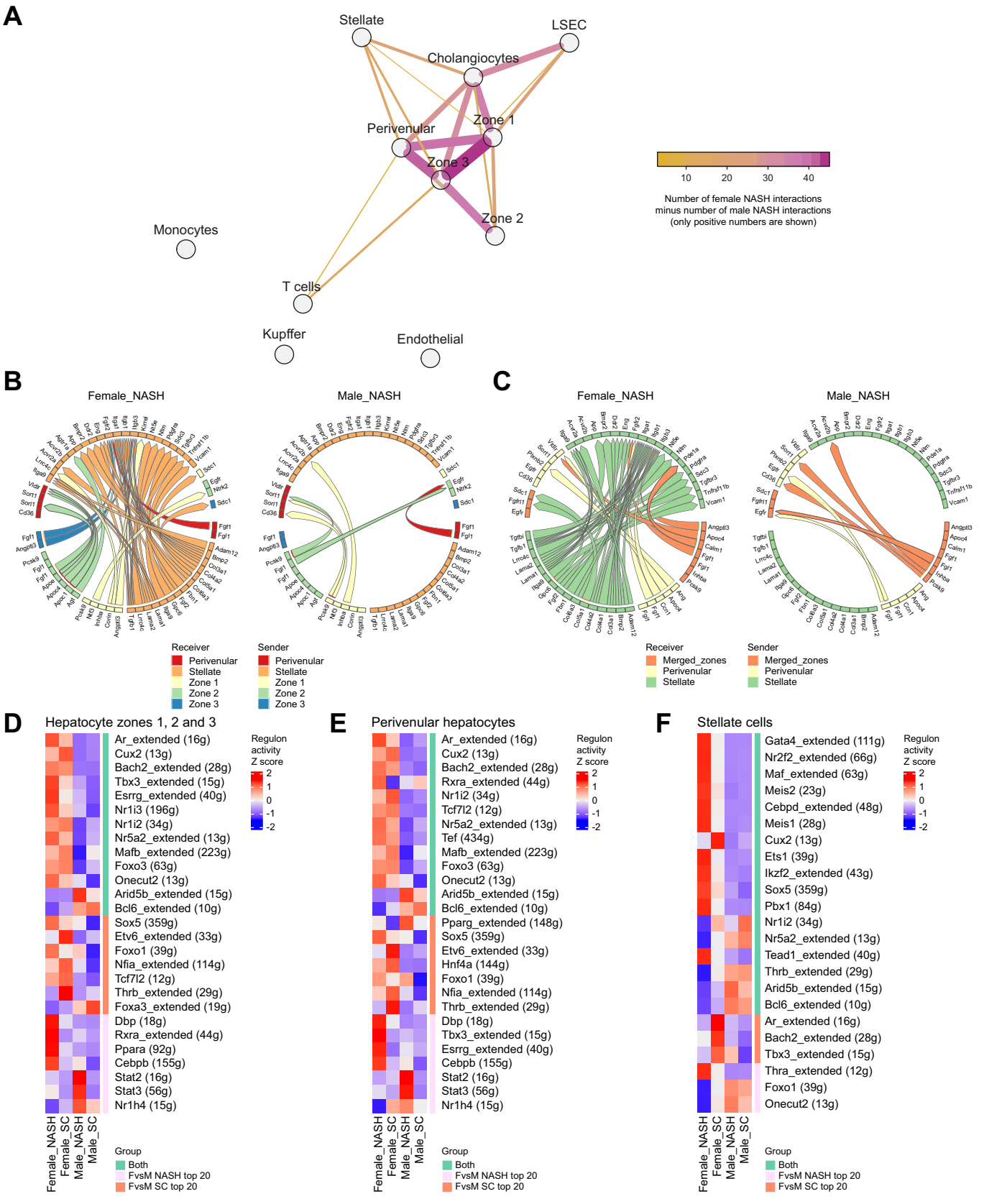

Fig. 6. Cell-cell communications in the liver in FPC-NASH diet. (A) Significant (*p* value <0.05) ligand-receptor interactions were identified using CellPhoneDB among all cell types in female FPC-NASH and male FPC-NASH. The network shows the differences in the number of significant interactions between female FPC-NASH and male FPC-NASH, showing connections only where positive numbers are found (*i.e.* with a larger number of interactions in females compared to males). Autocrine interactions are not shown. (B) Top 50 ligand-receptor interactions among hepatocyte subtypes and stellate cells, with the largest differences in signaling strength

predominantly expressed in stellate cells. In merged hepatocyte zones 1, 2 and 3 and in the individual hepatocyte zones 1, 2 and 3, there is an upregulation of genes involved in inflammation in female *vs.* male FPC-NASH-fed mice. In contrast, in SC-fed mice, very few differences between females *vs.* males were observed. Inflammation-related genes are expressed in stellate cells of all treatments relative to hepatocytes; yet, the overall pattern demonstrated even higher expression of these genes in female FPC-NASH.

Collectively, these findings reveal enrichment of genes and biological processes related to oxidative stress and inflammation in hepatocytes and stellate cells linked to MASLD/MASH in female *vs.* male mice fed FPC-NASH but not SC.

Cell-cell communications in the liver in FPC-NASH diet feeding

In addition to cell-intrinsic roles for hepatocytes and stellate cells in female and male mice in the response to FPC-NASH, it was important to determine if inter-cellular communications may contribute to MASLD/MASH-like pathologies. We employed CellPhoneDB[28] to identify ligand-receptor interactions between cell types within each condition. We compared these ligand-receptor interactions between conditions in the network illustrated in Fig. 6A. We subtracted the total number of ligand-receptor interactions in FPC-NASH-fed males from the total number of ligand-receptor interactions in FPC-NASH-fed females. Whenever this difference represented a positive number, a connection is included in the network. In this Figure, the connection color and weight represent the difference between females and males; hence the illustrated thick purple line indicates that there were at least 40 more interactions found between hepatocyte zones 1 and 3 in females *vs.* males, and that this enrichment of ligand-receptor interactions in females *vs.* males involves hepatocytes (zones 1, 2, and 3) and stellate cells, in addition to LSECs, T cells, cholangiocytes and perivenular hepatocytes, but not monocytes, Kupffer cells or endothelial cells. Based on these results and the collective data described above, we focused on the interactions between hepatocytes and stellate cells.

Although our findings to this point provide insight into the biological processes that differ between females *vs.* male mice fed FPC-NASH, they do not provide information on the nature of the upstream processes that control these responses. Hence, we employed MultiNicheNet[29] to investigate cell-cell communication. MultiNicheNet is distinct from CellPhoneDb in that it takes into account the differential expression of ligands, receptors and putative targets to prioritize interactions. Fig. 6B considers female *vs.* male individual hepatocyte zones 1, 2 and 3 interactions with stellate cells. We examined the top 50 ligand-receptor interactions found by MultiNicheNet and observed that most of these interactions occur in female *vs.* male FPC-NASH; with a substantial number of communications between hepatocytes and stellate cells and within stellate cells. The finding of increased cell-cell communication among hepatocytes and stellate cells in females relative to males fed FPC-NASH is consistent with results from CellPhoneDb. Analogous findings were observed when hepatocyte zones 1, 2, and 3 were merged (Fig. 6C).

Transcription factor regulation of liver transcriptome in FPC-NASH feeding

To identify the transcription factors that may regulate the liver transcriptome in female *vs.* male FPC-NASH-fed mice, we employed Single-Cell rEgulatory Network Inference and Clustering (SCENIC);[30] SCENIC infers transcription factor activity based on the expression patterns in their known targets. The term "regulon" is employed to denote a transcription factor and its target genes. We merged hepatocyte zones 1, 2 and 3 based on the evidence that the analysis of merged vs. individual hepatocyte zones 1, 2 and 3 yielded analogous results. To prioritize the results from SCENIC, we selected the top 20 regulons with the largest differences in activity between FPC-NASH-fed females *vs.* males, and SC-fed females *vs.* males in each of the merged hepatocyte zones 1, 2 and 3; perivenular hepatocytes; and stellate cells (Fig. 6D-F, respectively; Table S1). In the heatmaps, red colors indicate higher activity and the bar on the right indicates whether the regulon was identified in the top 20 regulons for FPC-NASH (pink vertical bar), SC (orange vertical bar), or both FPC-NASH and SC (green vertical bar).

To better understand how these regulons may be operative, we generated networks that illustrate the transcription factors connected with their target genes. Only target genes of the regulons that were also found to be differentially expressed in the snRNAseq data set between females *vs.* males are considered in the networks. A key question was the extent to which the processes underway in female *vs.* male merged hepatocyte zones 1, 2, and 3, perivenular hepatocytes, and stellate cells reflect an exacerbation of basal differences in the liver in FPC-NASH *vs.* SC, and/or the extent to which there are unique networks stimulated or inhibited by FPC-NASH. We generated distinct networks, and color highlighted the targets in the network based on their fold-change in females *vs.* males and further colored genes in the networks based on enriched functions (GO terms).

First, we considered merged hepatocyte zones 1, 2, and 3 and examined FPC-NASH-specific networks. Four regulons with higher activity were identified in females *vs.* males (*Dbp, Rxra, Ppara*, and *Cebpb*) and three regulons with higher activity were identified in males *vs.* females (*Stat2, Stat3* and *Nr1h4*) (Fig. 7A). When considering the differentially expressed target genes of these transcription factors, significant GO term enrichment analysis identifies three major functions:[1] hormone-mediated signaling;[2] alpha amino acid metabolic process; and[3] lipid metabolic stress (Fig. 7B; the full GO enrichment output for the network can be found in Table S1). Note that when comparing SC-fed

between female NASH and male NASH, as identified by MultiNichenet analysis using individual hepatocyte subtypes. (C) Top 50 ligand-receptor interactions among hepatocytes and stellate cells, with the largest differences in signaling strength between female NASH and male NASH, as identified by MultiNichenet analysis using merged hepatocyte zones. (D-F) Average regulon activity calculated by SCENIC for each condition, for the top 20 regulons with the largest difference in activity in female *vs.* male FPC-NASH, and female *vs.* male SC, in merged hepatocyte zones (D), perivenular hepatocytes (E), and stellate cells (F). Numbers between parentheses indicate the number of target genes that are part of the regulon. "Extended" indicates that the transcription factor binding motif for the regulon was inferred by SCENIC based on homology. LSEC, liver sinusoidal endothelial cell; SCENIC, Single Cell rEgulatory Network Inference and Clustering.

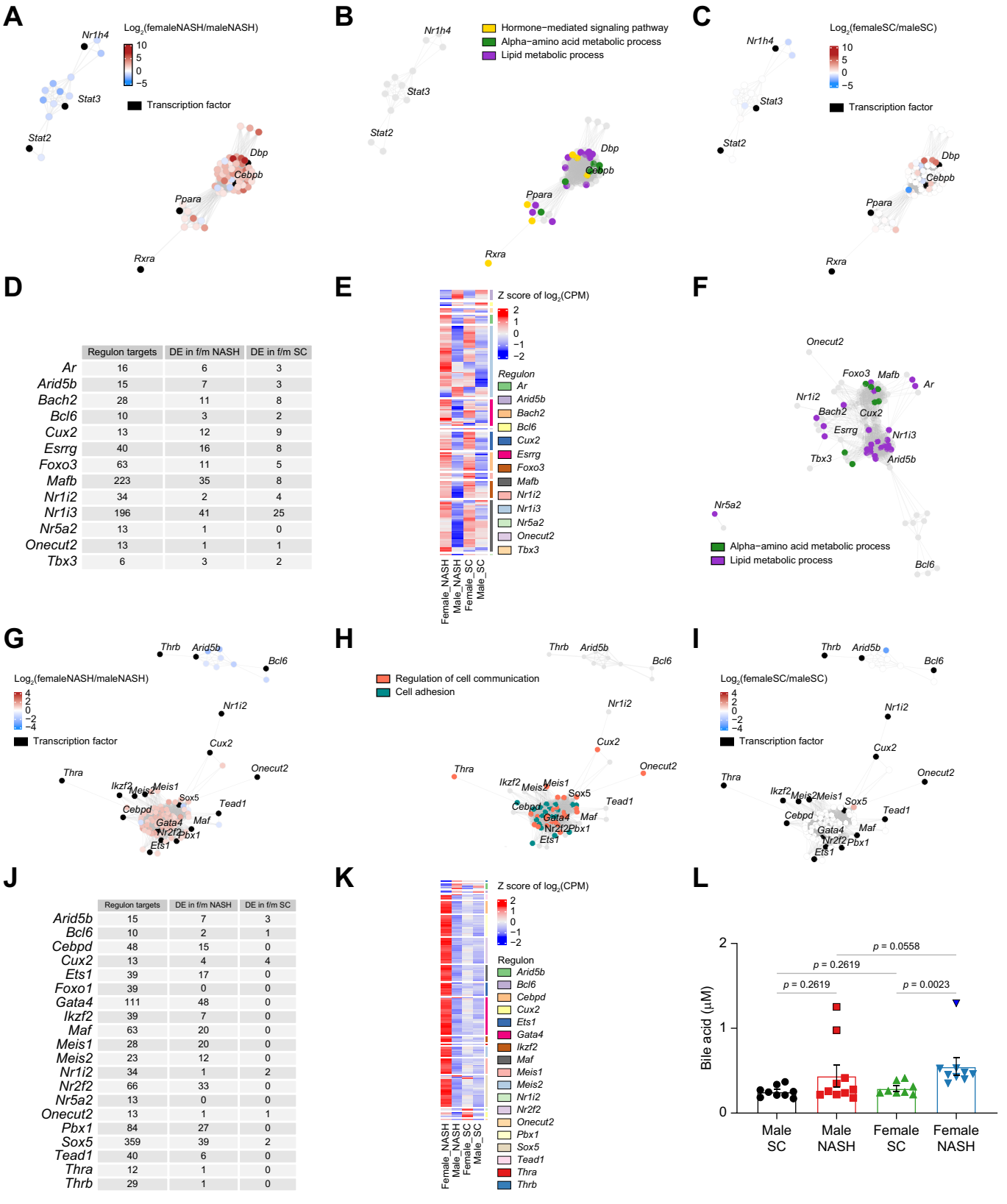

	Regulon targets	DE in f/m NASH	DE in f/m SC
Ar	16	6	3
Arid5b	15	7	3
Bach2	28	11	8
Bcl6	10	3	2
Cux2	13	12	9
Esrrg	40	16	8
Foxo3	63	11	5
Mafb	223	35	8
Nr1i2	34	2	4
Nr1i3	196	41	25
Nr5a2	13	1	0
Onecut2	13	1	1
Tbx3	6	3	2

Fig. 7. Examination of SCENIC regulons, target genes and networks in merged hepatocytes and stellate cells. (A) Network of top regulons identified only in female *vs.* male NASH in merged hepatocytes, using SCENIC analysis. The network shows transcription factors from the top regulons and their targets that were differentially expressed in female *vs.* male NASH merged hepatocytes in the pseudobulk differential expression analysis. Transcription factors are connected with their targets, and targets of the same regulon are connected with each other. Targets are colored by their fold-change in female *vs.* male NASH. (B) Network of top regulons

females *vs.* males, the sex-specific expression differences of regulon components were overall attenuated *vs.* the patterns noted in FPC-NASH (Fig. 7C).

To probe the contributions of diet, with respect to unique effects of FPC-NASH and/or enhancement of basal state (SC), we depicted transcription factors identified in the top 20 regulons of both FPC-NASH-fed females *vs.* males and SC-fed females *vs.* males; these are illustrated in Fig. 7D and include *Ar, Arid5b, Bach2, Bcl6, Cux2, Esrrg, Foxo3, Mafb, Nr1i2, Nr1i3, Nr5a2, Onecut2* and *Tbx3*. In nearly all cases (except *Nr1i2* and *Onecut2*), there are a greater number of predicted target genes of these regulons differentially expressed in females *vs.* males fed FPC-NASH compared to SC (Fig. 7D). The heatmap shown in Fig. 7E indicates the expression patterns (red *vs.* blue) for each of these regulons shown in Fig. 7D and F illustrates the network for these regulons, with targets colored by enriched GO terms. The enriched GO terms found among the top 20 regulons for both FPC-NASH and SC are very similar to the terms found for FPC-NASH alone, that is[1] alpha amino acid metabolic process; and[2] lipid metabolic stress (full GO term results are listed in Table S1). Experimental validation of these significantly differentially expressed target genes was sought in the deconvoluted Bulk RNAseq hepatocyte data set and in the Bulk RNAseq of the isolated hepatocytes. Of these targets, 11 were found to be differentially expressed in the isolated hepatocytes and 26 were found to be differentially expressed in the deconvoluted bulk RNAseq data set, when comparing females *vs.* males fed FPC-NASH.

With respect to the top 20 regulons unique to perivenular hepatocytes in FPC-NASH-fed mice, the findings were similar to those observed in the merged hepatocyte zones 1, 2, and 3; four regulons with higher activity were noted in female *vs.* male FPC-NASH (*Dbp, Tbx3, Esrrg*, and *Cebpb*) and the same three regulons with higher activity noted in the merged hepatocyte zones 1, 2, and 3 were noted in male *vs.* female FPC-NASH in perivenular hepatocytes (*Stat2* and *Stat1*) (Fig. 6E and Fig. S11A). When considering the differentially expressed target genes of these transcription factors, significant GO term enrichment analysis highlighted two of the same major biological processes identified above in merged hepatocyte zones 1, 2, and 3:[1] alpha amino acid metabolic process; and[2] lipid metabolic stress (Fig. S11B; full GO term output in Table S1). When comparing the expression changes in females *vs.* males fed FPC-NASH to those fed SC, we observe expression differences of a much smaller magnitude for SC (Fig. S11A,C).

As in the case of merged hepatocyte zones 1, 2, and 3, we depicted the target genes of the regulons identified in females *vs.* males for both FPC-NASH and SC in the perivenular hepatocytes; these are illustrated in Fig. S11D and include *Ar, Arid5b, Bach2, Bcl6, Cux2, Foxo3, Mafb, Nr1i2, Nr5a2, Onecut2, Rxra, Tcf7l2*, and *Tef*. We noted that in nearly all gene targets (except *Nr1i2* and *Rxra*), there is a greater number of target genes of these regulons differentially expressed in female *vs.* male FPC-NASH diet compared to SC diet (Fig. S11D). The heatmap shown in Fig. S11E indicates the expression patterns (red *vs.* blue) for each of these regulons. Figure S11F illustrates the network for these regulons with targets colored by enriched GO terms. The major enriched GO terms found for FPC-NASH and SC are very similar to the terms found for FPC-NASH alone, that is, metabolic process. Experimental validation of these significantly differentially expressed target genes was sought in the deconvoluted Bulk RNAseq hepatocyte data set and in the Bulk RNAseq of the isolated hepatocytes. Of the differentially expressed regulon targets identified in perivenular hepatocytes, nine were DEGs in the isolated hepatocytes and 11 were DEGs in the deconvoluted bulk RNAseq data set.

Collectively, these data suggest that the transcriptional programs in hepatocytes of females fed FPC-NASH differ from those of males fed FPC-NASH, due to a combination of 1) exacerbation of basal differences between females and males on SC and 2) the addition of unique regulons specific to FPC-NASH.

Lastly, we considered the stellate cells and generated the network shown in Fig. 7G that includes the regulons found in the top 20 of FPC-NASH and SC and those in the top 20 of only FPC-NASH. These include regulons for *Arid5b, Bcl6, Cebpd, Cux2, Ets1, Foxo1, Gata4, Ikzf2, Maf, Nr1i2, Meis1, Meis2, Nr1i2, Nr2f2, Nr5a2, Onecut2, Pbx1, Sox5, Tead1, Thra* and *Thrb* (Fig. 7G). When considering the differentially expressed target genes of these transcription factors, significant GO term enrichment analysis highlighted two major processes:[1] regulation of cell communication; and[2] cell adhesion (Fig. 7H; full

identified only in female *vs.* male NASH merged hepatocytes, with transcription factors and targets colored based on significant GO term enrichment (Biological Process; q-value <0.05). GO term enrichment was run jointly on all regulons. (C) Network of top regulons identified only in female *vs.* male NASH merged hepatocytes, with transcription factors and targets colored by their fold-change in female *vs.* male SC. (D) Number of DEGs in female *vs.* male NASH and female *vs.* male SC merged hepatocytes, for targets of the 13 regulons that are found in the top 20 regulons of both NASH and SC. (E) Normalized counts of DEGs in female *vs.* male NASH and female *vs.* male SC merged hepatocytes, for targets of the 13 regulons that are found in the top 20 regulons of both NASH and SC. (F) Network of 13 top regulons identified in both female *vs.* male NASH and female *vs.* male SC. The network shows transcription factors and targets that were DEGs in the pseudobulk differential expression analysis when comparing female *vs.* male NASH. Transcription factors and targets are colored based on significant GO term enrichment (biological process; adjusted *p* value <0.05). GO term enrichment was run jointly on all regulons. (G) Network showing the top 20 regulons identified using SCENIC in female *vs.* male NASH stellate cells. The networks show transcription factors, and targets that were DEGs in the pseudobulk differential expression analysis. Targets are colored by their fold-change in female *vs.* male NASH stellate cells. Transcription factors are connected with their targets, and targets of the same regulon are connected with each other. (H) Network showing the top 20 regulons identified using SCENIC in female *vs.* male NASH stellate cells, with transcription factors and targets colored based on significant GO term enrichment (biological process; adjusted *p* value <0.05). GO term enrichment was run jointly on all regulons. (I) Network showing the top 20 regulons identified using SCENIC in female *vs.* male NASH stellate cells, with transcription factors and targets colored by their fold-change in female *vs.* male SC. (J) Number of DEGs in female *vs.* male NASH and female *vs.* male SC stellate cells, for targets of the top 20 regulons identified using SCENIC in female *vs.* male NASH stellate cells. (K) Normalized counts of DEGs in female *vs.* male NASH and female *vs.* male SC stellate cells, for targets of the top 20 regulons identified using SCENIC in female *vs.* male NASH stellate cells. (L) Hepatic concentrations of total bile acids were measured after 16 weeks of diet in 10 mice per sex per diet. Statistical analyses were performed using the Wilcoxon rank-sum test. Multiple cohorts were employed for replication and to execute the biochemical studies reported in this figure. For group comparison, the Shapiro–Wilk normality test was conducted first for each group with prespecified significance level of 0.05, and if passed, the t test was implemented whereas the non-parametric Wilcoxon rank-sum test was used if normality was not established. False discovery rate-adjusted *p* values are reported in multiple hypothesis testing. Bile acid: Male NASH *vs.* Male SC, $p = 0.2619$; Female NASH *vs.* Female SC, $p = 0.0023$; Female SC *vs.* Male SC, $p = 0.2619$; and Female NASH *vs.* Male NASH, $p = 0.0558$. GO, Gene Ontology; SCENIC, Single-Cell rEgulatory Network Inference and Clustering.

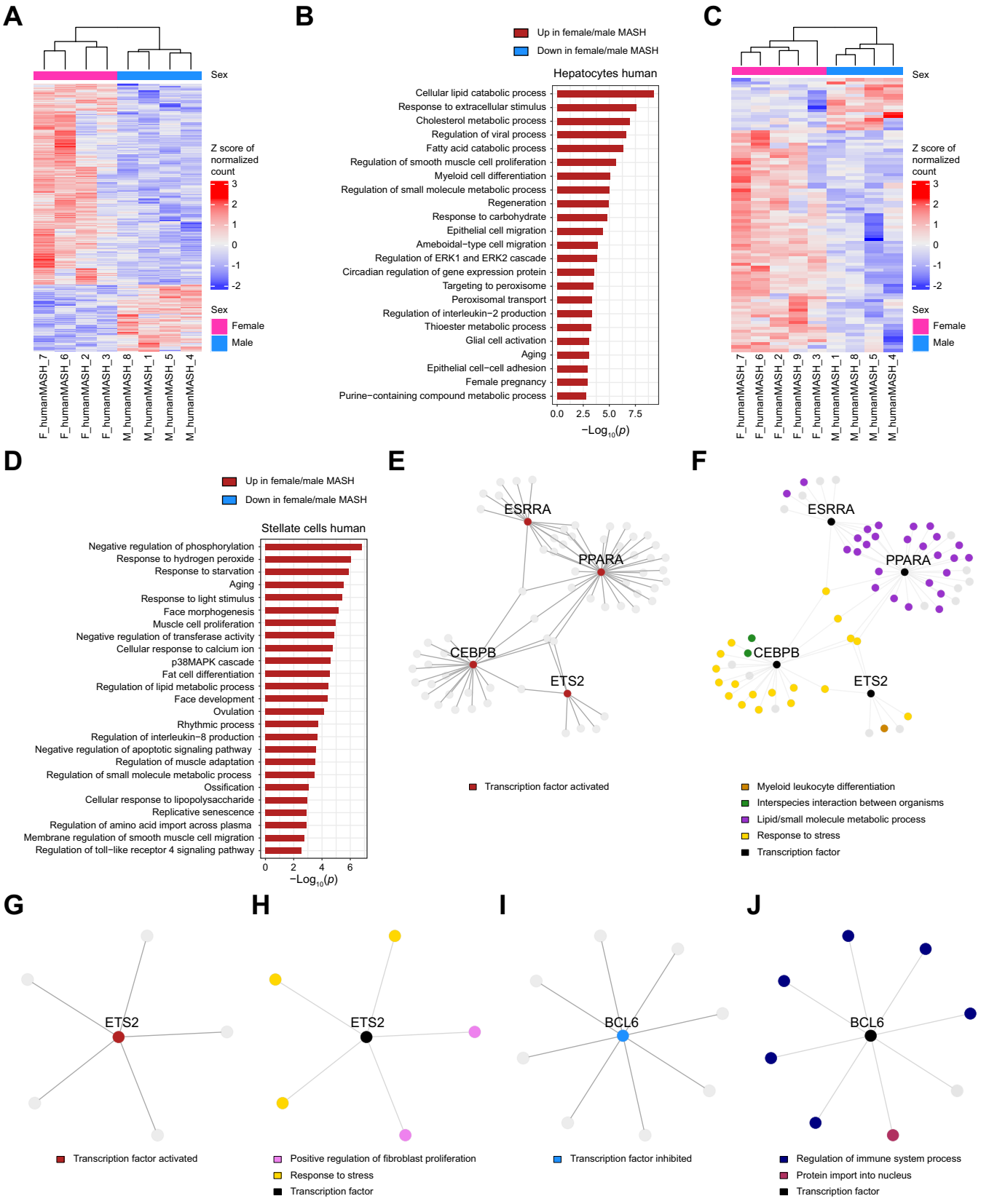

Fig. 8. Single-nucleus RNAseq and sex differences in human MASH. Data were obtained from male and female humans with MASH of single-nucleus RNAseq from a publicly available database (GSE212837)[54] and analyzed for sex differences. (A) Normalized counts of hepatocyte DEGs identified in a pseudobulk differential expression analysis, comparing female and male patients with MASH. Female n = 4; Male n = 4. DEGs were selected using *p* value <0.01. (B) Significantly enriched GO terms (biological process; q-value <0.05) for hepatocyte DEGs that were upregulated in female *vs.* male patients with MASH. No significant enrichment was found for

GO term output can be found in Table S1). When comparing females *vs.* males fed SC, only negligible differences in expression were observed (Fig. 7I). We depicted the number of target genes of these regulons in Fig. 7J and showed their expression patterns across all treatment groups in Fig. 7K. In all cases (except *Cux2, Foxo1, Nr5a2*, and *Onecut2*), there are a greater number of target genes of these regulons differentially expressed in females *vs.* males fed FPC-NASH (Fig. 7J,K). Experimental validation revealed that of the differentially expressed regulon targets identified in stellate cells in the snRNAseq, one was found to be differentially expressed in the isolated stellate cells and six were differentially expressed in the deconvoluted bulk RNAseq data set, when comparing females *vs.* males fed FPC-NASH.

Finally, we reasoned that predicted ligand-receptors interactions from MultiNiche Net data shown above (Fig. 6B), should be integrated, at least in part, with the findings of the in-depth SCENIC analysis. Fig. S12 shows that multiple regulon components (transcription factors or targets) from the SCENIC analysis are predicted targets of ligands identified by MultiNicheNet analysis. First, with respect to merged hepatocyte zones 1, 2, and 3, MultiNicheNet predicted that the Apoc4 ligand can regulate expression of the transcription factor AR, which was identified by SCENIC as having a higher activity in females *vs.* males. Second, with respect to perivenular hepatocytes, MultiNicheNet analysis predicted that within-hepatocyte signaling could regulate *Mafb* in females *vs.* males fed FPC-NASH, and *Mafb* was identified by SCENIC as having a higher activity in females *vs.* males. Third, with respect to stellate cells, MultiNicheNet analysis predicted roles for a number of the factors identified in the overall SCENIC analysis, including *Ets1, Maf, Ikzf2, Nr2f2, Pbx1* and *Sox5*.

Collectively, these data suggest that the transcription factors and their target genes in merged hepatocyte zones 1, 2, and 3 and perivenular hepatocytes contribute to the exacerbation of the disease phenotype in females *vs.* males fed FPC-NASH, which appear to be explained by exacerbation of basal differences together with the recruitment of distinct factors during FPC-NASH feeding. However, in stellate cells, the female *vs.* male enrichment appears to be accounted for largely through unique effects imbued by the FPC-NASH diet.

Metabolic flux and the FPC-NASH diet: Effect of sex

Differential gene expression analysis and GO term enrichment suggest that hepatocytes in female FPC-NASH very likely display a different metabolic profile compared to hepatocytes in male FPC-NASH. To investigate metabolic differences in more detail, a single-cell Flux Estimation Analysis (scFEA) was performed.[31] ScFEA employs a neural network to infer the relative activity of a set of metabolic reactions at the single-cell level, starting from single-cell or single-nucleus RNAseq data. The metabolic reactions are defined by their input and output metabolites. A higher flux value indicates a higher relative activity of a metabolic reaction, and increased conversion of the input metabolite to the output metabolite.

After running scFEA on the mouse single-cell RNAseq dataset, we compared metabolic flux through 168 reactions in the merged hepatocytes of FPC-NASH-fed females with the flux in FPC-NASH-fed males. We identified 87 reactions with significantly different flux (q-value <0.05 and |Cohen'sD| ≥0.5). Among these significant reactions, the strongest down-regulation in flux in female *vs.* male hepatocytes was the conversion of cholesterol to chenodeoxycholate (Cohen's D of −1.5), suggesting perturbations in bile acid metabolism in the female *vs.* male merged hepatocyte zones (Table S1). These data are illustrated in the volcano and density plots shown in Fig. S13A,B.

In light of these observations regarding bile metabolism, we reviewed the findings in Fig. 6D,E and noted that the activity of the regulon *Nr1h4* is lower in female *vs.* male FPC-NASH merged hepatocytes and perivenular hepatocytes. The regulons shown in Fig. 6D-E are the top 20 regulons with the largest absolute difference in activity between females and males (SC or FPC-NASH). To test whether this difference is statistically significant, we performed a Wilcoxon test to compare *Nr1h4* regulon activity between the different groups. In merged hepatocyte zones 1, 2 and 3, there is significantly lower activity in females *vs.* males for FPC-NASH (q-value = 3.85e-207) and SC (q-value = 8.12e-15). In perivenular hepatocytes, there is significantly lower activity in females *vs.* males for FPC-NASH (q-value = 1.61e-18) and no significant difference for SC. *Nr1h4* encodes the farnesoid X receptor (FXR), which plays seminal roles in the regulation of genes that control multiple facets of bile acid metabolism, such as synthesis, uptake, secretion and intestinal absorption.[32] We reviewed the results of significantly DEGs in the isolated hepatocytes of the FPC-NASH-fed mice and found that the expression of four genes known to be regulated by *Nr1h4* and that play critical roles in bile metabolism and secretion (*Slco1a1, Cyp7a1, Slc10a2* and *Cyb7b1*) were downregulated in female *vs.* male isolated primary hepatocytes, as was the expression of *Cyp7b1* and *Slco1a1* in hepatocytes in the snRNAseq data (Table S1). Of note, some of these genes were also downregulated in

downregulated DEGs. (C) Normalized counts of stellate cell DEGs identified in a pseudobulk differential expression analysis, comparing female and male patients with MASH. Female n = 5; Male n = 4. DEGs were selected using *p* values <0.01. (D) Significantly enriched GO terms (biological process; q-value <0.05) for stellate cell DEGs that were upregulated in female *vs.* male patients with MASH. No significant enrichment was found for downregulated DEGs. (E) Network showing transcription factors identified by IPA, that are activated in hepatocytes of female *vs.* male patients with MASH, and that are homologs or paralogs of transcription factors activated in female *vs.* male MASH hepatocytes or stellate cells in mice, based on SCENIC analysis. (F) Network from Fig. 8E with targets colored by significant GO term enrichment (biological process; q-value <0.05). GO term enrichment was run for each transcription factor and its targets separately. For each transcription factor and its targets, the top 2 most significant GO terms are shown in the network. (G) The transcription factor ETS2 is predicted to be activated in stellate cells of female *vs.* male patients with MASH, based on IPA upstream analysis. The network shows ETS2 and its predicted targets from the female *vs.* male DEGs in patients with MASH. (H) ETS2 targets are colored by significant GO term enrichment (biological process; q-value <0.05). The top two most significant GO terms are shown in the network. (I) The transcription factor BCL6 is predicted to be inhibited in stellate cells of female *vs.* male patients with MASH, based on IPA upstream analysis. The network shows BCL6 and its predicted targets from the female *vs.* male DEGs in patients with MASH. (J) BCL6 targets are colored by significant GO term enrichment (Biological Process; q-value <0.05). The top two most significant GO terms are shown in the network. DEGs, differentially expressed genes; GO, Gene Ontology.

female *vs.* male hepatocytes in mice fed SC, suggesting endogenous sex-dependent differences in bile metabolism, which may be exacerbated by FPC-NASH.

Finally, we measured total bile acid content in the livers of the mice under study. Although there were no significant differences in total bile acid content in the livers of male FPC-NASH- *vs.* SC-fed mice (p = 0.2619), total bile acid content was significantly higher in the livers of female FPC-NASH- *vs.* SC-fed mice (p = 0.0023; Fig. 7L). Furthermore, the livers of female FPC-NASH-fed mice displayed higher total bile acid content compared to male FPC-NASH-fed mice (p = 0.0558; Fig. 7L).

Sex differences in human MASH

To assess the relevance of our mouse model findings to human MASH, we analyzed a publicly available data set of snRNAseq (GSE212837) from four males and five females with MASH. This data set only contained two control female and one control male liver, which was not suitable for analysis. Although the human cases displayed varying durations of disease, fibrosis and MASH scores, our analysis nevertheless identified common elements between the human and mouse data sets.

Beginning with hepatocytes, 434 genes were differentially expressed between female and male patients with MASH (p ≤0.01) (Fig. 8A) (Table S4). The enrichment of GO terms in females *vs.* males with MASH was similar to that in female *vs.* male FPC-NASH-fed mice, including lipid and carbohydrate metabolism, such as cellular lipid catabolic process, cholesterol metabolic process, fatty acid catabolic process, response to carbohydrate, thioester metabolic process, and purine containing compound metabolic process (Fig. 8B). Analogous to findings in female *vs.* male FPC-NASH-fed mice, numerous GO terms enriched for inflammation were noted in human females *vs.* males with MASH: regulation of viral process, myeloid cell differentiation, and regulation of interleukin-2 production (Fig. 8B). Genes and GO terms related to sex-dependent processes were not prominent in the human data set, except for female pregnancy.

In the case of stellate cells, 89 genes were differentially expressed between female and male patients with MASH (p ≤0.01) (Fig. 8C). Enriched GO terms in females *vs.* males with MASH related to tissue reorganization were identified: face morphogenesis, muscle cell proliferation, fat cell differentiation, face development, regulation of muscle adaptation, ossification, and regulation of smooth muscle cell migration (Fig. 8D). Other GO terms related to lipid metabolism, oxidative stress and inflammation were enriched in the female *vs.* male MASH stellate cells: response to hydrogen peroxide, regulation of lipid catabolic process, regulation of interleukin-8 production, cellular response to lipopolysaccharide, and regulation of Toll-like receptor 4 pathway (Fig. 8D).

To identify potential overarching transcriptional regulators of the DEGs identified in human females *vs.* males with MASH, we performed SCENIC analysis, but noted that the regulon activity varied considerably from patient to patient. Hence, we employed Ingenuity Pathway Analysis (IPA) as an alternative method to identify potential upstream regulators based on DEG sets.[33] IPA "upstream analysis" results from merged hepatocyte zones and stellate cells were filtered to retain only transcription regulators and ligand-dependent nuclear receptors with significant (p <0.05) activation or inhibition in females *vs.* males with MASH.

We examined the merged human hepatocyte zones and generated a network by connecting transcription factors with their predicted targets, and by connecting targets of the same transcription factor(s) with each other. The transcription factors of interest were selected based on their having homologs or paralogs that were shown to be activated in female *vs.* male FPC-NASH-fed mice (Figs 6,7). This network uncovered transcriptional regulatory roles for ESRRA, PPARA, CEBPB and ETS2 (Fig. 8E). Next, we examined GO pathway term enrichment for each transcription factor and its targets separately. For each transcription factor and its targets, the top two most significant GO terms were selected for display in the network. In the merged hepatocyte zones, we identified the following enrichment terms for female *vs.* male MASH, which were consistent with those identified in the FPC-NASH mice: myeloid leukocyte differentiation, interspecies interaction between organisms, lipid and small molecule metabolic process, and response to stress (Fig. 8F).

We performed the scFEA on the human snRNAseq dataset and flux through 168 reactions was compared between hepatocytes of females and males with MASH. We identified 72 reactions with significantly different flux (q-value <0.05 and | Cohen'sD| ≥0.5). Among these is the conversion of cholesterol to chenodeoxycholate, which was significantly downregulated in female MASH hepatocytes relative to male MASH hepatocytes, with a Cohen's D of –0.7, analogous to our observations in mice (Fig. S13C,D).

Lastly, we examined stellate cells. As shown in Fig. 8G, the transcription factor ETS2 was activated in female *vs.* male patients with MASH; ETS1 was identified in the female *vs.* male FPC-NASH-fed mice. The two most significant GO terms found for the ETS2 network are positive regulation of fibroblast proliferation and response to stress, which were analogous to those identified in mice (Fig. 8H). In addition to activated transcription factors in stellate cells in human MASH, one factor was found to be inhibited, BCL6 (Fig. 8I), The two most significant GO terms found for the BCL6 network are regulation of immune cell process and protein import into the nucleus (Fig. 8J). For both hepatocytes and stellate cells, the full GO term enrichment for all networks may be found in Table S4.

Discussion

In summary, this study reveals significant sexual dimorphism in the response of C57BL/6J mice to the FPC-NASH diet over 16 weeks. While both sexes developed obesity, increased adiposity, glucose and insulin intolerance, and hyperlipidemia, female mice exhibited more severe hepatic steatosis, inflammation, and fibrosis compared to their male counterparts. A key question was the extent to which the findings in female *vs.* male FPC-NASH diet-fed mice were accounted for by exacerbation of basal sex-dependent gene expression programs in the liver (SC) and/or through unique regulatory factors up- or down-regulated in female *vs.* male mice fed FPC-NASH. We uncovered that in both the merged hepatocyte zones 1, 2, and 3 and perivenular hepatocytes, but to a lesser degree in stellate cells, female *vs.* male differential activation of regulons was characterized both by exacerbation of basal differences in the liver, as well as by FPC-NASH-specific re-programming (Fig. 6D-F). In the merged hepatocyte zones 1, 2 and 3, differences in metabolic pathways in the response to FPC-NASH were noted

between sexes, and, in particular, female hepatocytes displayed a more exuberant metabolic response. Furthermore, male *vs.* female hepatocytes displayed upregulation of pathways related to wound healing and thrombosis/hemostasis, which suggests enhanced tissue remodeling *vs.* female hepatocytes in FPC-NASH *vs.* SC.

Male stellate cells uniquely upregulated pathways associated with inflammation and balanced extracellular matrix organization. Notably, pathways related to coagulation, complement, and plasminogen were selectively activated in males, suggesting mechanisms to limit excessive extracellular matrix production. Furthermore, male stellate cells showed downregulation of amino acid metabolism pathways, potentially indicating reduced extracellular matrix production. These changes were not observed in female stellate cells.

Collectively, these findings suggest that male mice may possess more robust defensive mechanisms against excessive metabolism and extracellular matrix expansion in response to the FPC-NASH diet. This could potentially explain the less severe liver pathology observed in male mice despite similar metabolic challenges. Among the regulons affected in FPC-NASH- and SC-fed mice were factors known to be regulated in a sex-specific manner. This is not surprising, as it is established in both mouse and human livers that regulation of gene expression is, in part, sex-dependent.[34,35] In human livers, for example, 1,249 sex-biased genes were identified, 70% of which were shown to display higher expression in females. Analysis of the top biological functions and diseases that were significantly enriched in sex-biased genes include lipid metabolism and cardiovascular disease, among others.[34]

Examination of some of the key regulons enriched in female *vs.* male mice yielded insights into the means by which FPC-NASH diet affected expression of basal sex-biased gene expression patterns. First, our studies revealed that the AR (androgen receptor) regulon was upregulated in female vs. male merged hepatocyte zones and perivenular hepatocytes in FPC-NASH and in SC. Consistent with these concepts, we found that selectively in female mice, FPC-NASH diet resulted in increased plasma concentrations of testosterone *vs.* SC and, indeed, female mice displayed exacerbated liver injury in response to FPC-NASH diet *vs.* males. While hepatic steatosis is associated with reductions in testosterone in men, androgens may promote hepatic steatosis in females, while endogenous estradiol is protective in the liver in both sexes.[36] Studies in mice showed that administration of inhibitors of the AR (EPI-001) were protective in male C57BL/6J mice fed a high-fat/high-sugar diet.[37] However, it was shown that hepatic deletion of AR in male mice fed a high-fat diet resulted in severe steatosis and insulin resistance, suggestive of protective roles for AR in male mice.[38] In marked contrast, hepatic deletion of AR in female mice fed the high-fat diet resulted in greatly reduced steatosis and injury, suggesting deleterious roles for AR in female mice.[38] Hence, in females, treatment of MASH with AR inhibitors may be worthy of testing.

In contrast to regulons enriched in female *vs.* male livers for both FPC-NASH and SC, a number of regulons were identified that were uniquely enriched in FPC-NASH-fed female *vs.* male livers, both in merged hepatocyte zones 1, 2, and 3 and in perivenular hepatocytes. Interestingly, these regulons were largely not classically identified as sex-biased genes, but, rather, they were strongly linked to lipid and bile metabolism, such as RXRA, PPARA, CEBPB, NR1H4, STAT2 and STAT3 (Fig. 6D,E).[39–44] Additional data analyses in our study pinpointed potential roles for NR1H4 (FXR). In both human and mouse hepatocytes, the scFEA algorithm suggested a significant downregulation of "Cholesterol-Chenodeoxycholate" metabolism. Our findings concur with this result. First, we found that total bile acid content was significantly higher in female FPC-NASH *vs.* female SC livers and was higher in female *vs.* male FPC-NASH livers. Second, gene expression analyses of isolated primary hepatocytes and merged hepatocyte zones in the snRNA-seq data set suggested a downregulation of multiple FXR-dependent genes that regulate bile metabolism, including the process of secretion (*Cyp7a1, Cyp7b1, Slco1a1* and *Slc10a2*). Indeed, it is established that diminished secretion of bile acids may result in hepatic inflammation, at least in part through Toll-like receptor 9 and chemokines.[45] Further, such persistent inflammation has been associated with increased fibrosis.[46] In this context, it is plausible that exaggerated perturbations in bile metabolism and secretion in female *vs.* male hepatocytes may contribute to the significantly greater steatosis, steatohepatitis and fibrosis in MASH. Hence, treatments to stimulate FXR, such as obeticholic acid or GW4064 might be worthy of testing, particularly in female MASH[47,48].

In addition, our data analyses suggest that stellate cells also contribute to sex-dependent effects in FPC-NASH (Fig. 4D). Analysis of regulons revealed that female *vs.* male-enriched stellate cell regulons were evident especially in FPC-NASH (THRA, FOXO1 and ONECUT2), which were related to immune, lipid metabolism and cell structure pathways (Fig. 6F). Specifically, the THRA (thyroid hormone receptor) is associated with hepatic steatosis, as genetic deletion of THRA protects against high-fat diet-induced hepatic steatosis and insulin resistance.[49] THRA was significantly upregulated only in females fed FPC-NASH; in all other conditions, its expression was reduced. Of note, a recent study showed that 52 weeks administration of two different doses of resmetirom, an inhibitor of human THRB, resulted in at least one stage improvement of "NASH" resolution and improvement in liver fibrosis.[50] Overall, among all treatment groups, between 43.5% and 44.5% of the participants identified as male in that study.

In addition, beyond THRs, FOXO1 expression in stellate cells is protective against hepatic fibrosis.[51] In our analysis, FOXO1 was uniquely downregulated in FPC-NASH-fed females *vs.* all other groups. FOXO1 has been linked to inhibition of proliferation and transdifferentiation of stellate cells.[51] Finally, ONECUT2 has been associated with numerous types of liver injury, such as carcinoma and MASLD/MASLD.[52,53]

Beyond the cell-intrinsic impact of DEGs and regulons and their target genes, many of which were experimentally validated in our independent bulk RNAseq of whole liver and of isolated primary hepatocytes and stellate cells, inter-cellular and ligand-receptor communications in the liver have been associated with advanced fibrosis. Our CellPhonedb and MultiNicheNet findings (Fig. 6A-C) revealed that most of the top 50 interactions were largely observed in FPC-NASH-fed females *vs.* males, including numerous communications between hepatocytes and stellate cells, and directly between stellate cells. Yet, unlike in the female mice, in the male mice, there were no stellate cell-stellate cell interactions identified among the top 50 interactions (Fig. 6B,C). Recent work from the Friedman laboratory[54]

employing snRNAseq identified, through CellPhoneDB, the emergence of an autocrine circuit in multiple cell-cell communication networks, including between activated stellate cells in advanced stages of fibrosis. That work did not specifically address potential sex differences in these networks in the mouse model. Further, in that study, the diet employed was different from that used here. Those authors used a Western diet (21.2% fat and 1.25% cholesterol) together with fructose and glucose in the drinking water. However, in addition, the mice also received injections of carbon tetrachloride, a potent inducer of liver fibrosis.[54] Importantly, in the present study, we demonstrated that even without carbon tetrachloride, only the female mice, but not male mice fed FPC-NASH diet, displayed evidence of stellate cell-stellate cell communications in fibrosis.

We acknowledge the limitations of the present work: first, it will be essential to probe potential roles for female *vs.* male gut microbiome-host interactions in the pathogenesis of MASLD/MASH; second, expanding the studies to other models of MASH will be informative; third, the use of gonadectomy in male and female mice may aid in dissecting the precise contributions of estrogen and testosterone; fourth, as it is plausible that all of the distinct components of the FPC-NASH diet contributed individually or in a synergistic manner to the observed metabolic dysfunction and derangements in liver homeostasis, which were exacerbated in females, future studies might consider inclusion of more detailed dietary histories in male and female patients with MASH; and sixth, now that the *transcriptional* basis of the sex differences has been studied in great detail, the next steps, especially those aiming to identify trackable biomarkers of these sex differences in MASH, include the use of metabolomics, lipidomics and proteomics assays on plasma and, possibly, urine to begin to identify biomarker panels for MASH and, particularly, highlight areas for therapeutic interruption of the pro-fibrosis pathways, which may be sex-specific.

Taken together, our studies employed biochemical, pathological, molecular, and bioinformatics techniques to identify distinct within-sex and between sex differences in transcriptional mechanisms in mouse liver cells. Many of these findings were recapitulated, at least in part, in human female *vs.* male patients with MASH. Beyond transcriptional mechanisms, metabolic flux experiments implicate impaired bile acid metabolism in exacerbation of these processes in female *vs.* male FPC-NASH-fed mice. Given that there are limited therapies for MASH and that preclinical studies are reported to include both sexes in only 5% of published studies,[16] our work underscores the imperative to test both males and females in preclinical studies and in clinical trials. We suggest that the present detailed molecular landscape of female *vs.* male livers in MASLD/MASH supports that sex-specific therapeutic targets, such as antagonizing the AR and/or enhancing bile metabolism and secretion, particularly in females, may be worthy of testing.

Affiliations

[1]*Diabetes Research Program, Department of Medicine, New York University Grossman School of Medicine Langone Health, New York, NY 10016, USA;* [2]*NYU Cardiovascular Research Center, Leon H. Charney Division of Cardiology, New York University Grossman School of Medicine Langone Health, New York, NY 10016, USA;* [3]*Departments of Population Health (Biostatistics) and Environmental Medicine, New York University Grossman School of Medicine Langone Health, New York, NY 10016, USA;* [4]*Department of Microbiology, New York University Grossman School of Medicine Langone Health, New York, NY 10016, USA;* [5]*Department of Pathology, New York University Grossman School of Medicine Langone Health, New York, NY 10016, USA*

Acknowledgments

The authors gratefully acknowledge the expert assistance of Ms. Latoya Woods of the Diabetes Research Program, Department of Medicine, New York University Grossman School of Medicine, in the preparation of this manuscript.

Abbreviations

ALT, alanine aminotransferase; AR, androgen receptor; AST, aspartate aminotransferase; DEG, differentially expressed genes; FPC, fructose-palmitate-cholesterol; FXR, farnesoid X receptor; GO, gene ontology; IPA, Ingenuity Pathway Analysis; MASH, metabolic dysfunction-associated steatohepatitis; MASLD, metabolic syndrome-associated steatotic liver disease; NASH, non-alcoholic steatohepatitis; QC, quality control; SC, standard chow; SCENIC, Single-Cell rEgulatory Network Inference and Clustering; UMAP, uniform manifold approximation and projection.

Financial support

1P01HL131481 (AMS, RR, KJM, MJG and EAF); American Heart Association Strategically Focused Network on Obesity 17SFRN33490004 (AMS); US Public Health Service 1P01HL146367 (AMS, RR), and 5K01DK120782-02 (HHR); and the NYU Histology Core and the Genome Technology Core, which is partially supported by New York University Cancer Institute Cancer Center Support Grant 5P30CA016087-31. Support was also provided from the Diabetes Research Program, New York University Grossman School of Medicine.

Conflict of interest

AMS and RR have patents and patent applications (New York University Grossman School of Medicine) that have been submitted or published that are not directly related to the work detailed in this manuscript. The other authors declared no conflict of interest.

Please refer to the accompanying ICMJE disclosure forms for further details.

Authors' contributions

LA, SD and AMS designed the research and analyzed data. LA, SD, RAW, KM, RH, and HHR performed experiments and analyzed data. NDT performed all of the pathological analysis of liver tissue. EB and SD performed the bioinformatics analyses. BZ and HL performed data and statistical analyses. MJG, RR, KJM, EAF and NDT contributed analytically and intellectually to the interpretation of data. LA, RAW, MBM, KM, RH, HHR, NDT, EB, BZ, HL, MJG, RR, KM, and EAF reviewed the data and edited the manuscript. AMS, KJM, and EAF secured funding for the study. AMS and SD wrote and edited the original draft of the manuscript. AMS conceived studies, designed the research, supervised the design and completion of experiments, analyzed data, and wrote and edited the final manuscript.

Data availability statement

All primary data associated with this study are present in the paper or the Supplementary Materials. All of the single-nucleus RNA sequencing, bulk RNA sequencing and spatial transcriptomics data were submitted to GEO with accession number GSE256505. Any materials reported in this research are available through a material transfer agreement (MTA) with New York University Grossman School of Medicine.

Supplementary data

Supplementary data to this article can be found online at https://doi.org/10.1016/j.jhepr.2024.101222.

References

Author names in bold designate shared co-first authorship

[1] Riazi K, Azhari H, Charette JH, et al. The prevalence and incidence of NAFLD worldwide: a systematic review and meta-analysis. Lancet Gastroenterol Hepatol 2022;7:851–861.

[2] Duell PB, Welty FK, Miller M, et al. Nonalcoholic fatty liver disease and cardiovascular risk: a scientific statement from the American Heart association. Arterioscler Thromb Vasc Biol 2022;42:e168–e185.

[3] Maier S, Wieland A, Cree-Green M, et al. Lean NAFLD: an underrecognized and challenging disorder in medicine. Rev Endocr Metab Disord 2021;22:351–366.

[4] Burra P, Bizzaro D, Gonta A, et al. Clinical impact of sexual dimorphism in non-alcoholic fatty liver disease (NAFLD) and non-alcoholic steatohepatitis (NASH). Liver Int 2021;41:1713–1733.

[5] Hashimoto E, Tokushige K. Prevalence, gender, ethnic variations, and prognosis of NASH. J Gastroenterol 2011;46(Suppl 1):63–69.

[6] Balakrishnan M, Patel P, Dunn-Valadez S, et al. Women have a lower risk of nonalcoholic fatty liver disease but a higher risk of progression vs men: a systematic review and meta-analysis. Clin Gastroenterol Hepatol 2021;19:61–71.e15.

[7] Ilyas F, Ali H, Patel P, et al. Increasing nonalcoholic fatty liver disease-related mortality rates in the United States from 1999 to 2022. Hepatol Commun 2023;7.

[8] Eng PC, Forlano R, Tan T, et al. Non-alcoholic fatty liver disease in women - current knowledge and emerging concepts. JHEP Rep 2023;5:100835.

[9] White JS. Straight talk about high-fructose corn syrup: what it is and what it ain't. Am J Clin Nutr 2008;88:1716s–1721s.

[10] Buck AW. High fructose corn syrup. In: Nabors LO, editor. Alternative sweeteners. New York: Marcel Dekker; 2001. p. 391–411.

[11] Daniels LA. Coke, Pepsi to use more corn syrup. New York Times 1984 November 7. 1984; Sect. D. Page 6.

[12] Ma J, Fox CS, Jacques PF, et al. Sugar-sweetened beverage, diet soda, and fatty liver disease in the Framingham Heart Study cohorts. J Hepatol 2015;63:462–469.

[13] Stanhope KL, Schwarz JM, Keim NL, et al. Consuming fructose-sweetened, not glucose-sweetened, beverages increases visceral adiposity and lipids and decreases insulin sensitivity in overweight/obese humans. J Clin Invest 2009;119:1322–1334.

[14] Hieronimus B, Medici V, Bremer AA, et al. Synergistic effects of fructose and glucose on lipoprotein risk factors for cardiovascular disease in young adults. Metabolism 2020;112:154356.

[15] Gallage S, Avila JEB, Ramadori P, et al. A researcher's guide to preclinical mouse NASH models. Nat Metab 2022;4:1632–1649.

[16] **Im YR**, **Hunter H**, **de Gracia Hahn D**, **Duret A**, et al. A systematic review of animal models of NAFLD finds high-fat, high-fructose diets most closely resemble human NAFLD. Hepatology 2021;74:1884–1901.

[17] Wang X, Zheng Z, Caviglia JM, et al. Hepatocyte TAZ/WWTR1 promotes inflammation and fibrosis in nonalcoholic steatohepatitis. Cell Metab 2016;24:848–862.

[18] Kleiner DE, Brunt EM, Van Natta M, et al. Design and validation of a histological scoring system for nonalcoholic fatty liver disease. Hepatology 2005;41:1313–1321.

[19] Vega GL, Grundy SM. Metabolic risk susceptibility in men is partially related to adiponectin/leptin ratio. J Obes 2013;2013:409679.

[20] Frühbeck G, Catalán V, Rodríguez A, et al. Adiponectin-leptin ratio: a promising index to estimate adipose tissue dysfunction. Relation with obesity-associated cardiometabolic risk. Adipocyte 2018;7:57–62.

[21] Hao Y, Hao S, Andersen-Nissen E, et al. Integrated analysis of multimodal single-cell data. Cell 2021;184:3573–3587.e3529.

[22] **Halpern KB**, **Shenhav R**, Matcovitch-Natan O, et al. Single-cell spatial reconstruction reveals global division of labour in the mammalian liver. Nature 2017;542:352–356.

[23] Rives C, Fougerat A, Ellero-Simatos S, et al. Oxidative stress in NAFLD: role of nutrients and food contaminants. Biomolecules 2020;10.

[24] Allameh A, Niayesh-Mehr R, Aliarab A, et al. Oxidative stress in liver pathophysiology and disease. Antioxidants (Basel) 2023;12.

[25] Petagine L, Zariwala MG, Patel VB. Non-alcoholic fatty liver disease: immunological mechanisms and current treatments. World J Gastroenterol 2023;29:4831–4850.

[26] Ma DW, Ha J, Yoon KS, et al. Innate immune system in the pathogenesis of non-alcoholic fatty liver disease. Nutrients 2023;15.

[27] Vachliotis ID, Polyzos SA. The role of tumor necrosis factor-alpha in the pathogenesis and treatment of nonalcoholic fatty liver disease. Curr Obes Rep 2023;12:191–206.

[28] Efremova M, Vento-Tormo M, Teichmann SA, et al. CellPhoneDB: inferring cell-cell communication from combined expression of multi-subunit ligand-receptor complexes. Nat Protoc 2020;15:1484–1506.

[29] Browaeys R, Gilis J, Sang-Aram C, et al. MultiNicheNet: a flexible framework for differential cell-cell communication analysis from multi-sample multi-condition single-cell transcriptomics data. bioRxiv 2023;2023. 2006.2013.544751.

[30] Aibar S, González-Blas CB, Moerman T, et al. SCENIC: single-cell regulatory network inference and clustering. Nat Methods 2017;14:1083–1086.

[31] **Alghamdi N**, **Chang W**, Dang P, et al. A graph neural network model to estimate cell-wise metabolic flux using single-cell RNA-seq data. Genome Res 2021;31:1867–1884.

[32] Tu H, Okamoto AY, Shan B. FXR, a bile acid receptor and biological sensor. Trends Cardiovasc Med 2000;10:30–35.

[33] Krämer A, Green J, Pollard Jr J, et al. Causal analysis approaches in ingenuity pathway analysis. Bioinformatics 2014;30:523–530.

[34] Zhang Y, Klein K, Sugathan A, et al. Transcriptional profiling of human liver identifies sex-biased genes associated with polygenic dyslipidemia and coronary artery disease. PLoS One 2011;6:e23506.

[35] Mode A, Gustafsson JA. Sex and the liver - a journey through five decades. Drug Metab Rev 2006;38:197–207.

[36] Grossmann M, Wierman ME, Angus P, et al. Reproductive endocrinology of nonalcoholic fatty liver disease. Endocr Rev 2019;40:417–446.

[37] Wang S, Li X, Xu W, et al. Amelioration of hepatic steatosis by the androgen receptor inhibitor EPI-001 in mice and human hepatic cells is associated with the inhibition of CYP2E1. Int J Mol Sci 2022;23.

[38] Dean AE, Reichardt F, Anakk S. Sex differences feed into nuclear receptor signaling along the digestive tract. Biochim Biophys Acta Mol Basis Dis 2021;1867:166211.

[39] Makarova E, Kazantseva A, Dubinina A, et al. The same metabolic response to FGF21 administration in male and female obese mice is accompanied by sex-specific changes in adipose tissue gene expression. Int J Mol Sci 2021;22.

[40] Dong Q, Kuefner MS, Deng X, et al. Sex-specific differences in hepatic steatosis in obese spontaneously hypertensive (SHROB) rats. Biol Sex Differ 2018;9:40.

[41] Ballester M, Ramayo-Caldas Y, Revilla M, et al. Integration of liver gene co-expression networks and eGWAs analyses highlighted candidate regulators implicated in lipid metabolism in pigs. Sci Rep 2017;7:46539.

[42] Staiger J, Lueben MJ, Berrigan D, et al. C/EBPbeta regulates body composition, energy balance-related hormones and tumor growth. Carcinogenesis 2009;30:832–840.

[43] Shrivastava S, Meissner EG, Funk E, et al. Elevated hepatic lipid and interferon stimulated gene expression in HCV GT3 patients relative to non-alcoholic steatohepatitis. Hepatol Int 2016;10:937–946.

[44] Gunduz F, Aboulnasr FM, Chandra PK, et al. Free fatty acids induce ER stress and block antiviral activity of interferon alpha against hepatitis C virus in cell culture. Virol J 2012;9:143.

[45] Cai SY, Ouyang X, Chen Y, et al. Bile acids initiate cholestatic liver injury by triggering a hepatocyte-specific inflammatory response. JCI Insight 2017;2:e90780.

[46] Jalan-Sakrikar N, De Assuncao TM, Shi G, et al. Proteasomal degradation of enhancer of zeste homologue 2 in cholangiocytes promotes biliary fibrosis. Hepatology 2019;70:1674–1689.

[47] Cao Y, Xiao Y, Zhou K, et al. FXR agonist GW4064 improves liver and intestinal pathology and alters bile acid metabolism in rats undergoing small intestinal resection. Am J Physiol Gastrointest Liver Physiol 2019;317:G108–g115.

[48] Zhang Y, LaCerte C, Kansra S, et al. Comparative potency of obeticholic acid and natural bile acids on FXR in hepatic and intestinal in vitro cell models. Pharmacol Res Perspect 2017;5.

[49] Jornayvaz FR, Lee HY, Jurczak MJ, et al. Thyroid hormone receptor-α gene knockout mice are protected from diet-induced hepatic insulin resistance. Endocrinology 2012;153:583–591.

[50] Harrison SA, Bedossa P, Guy CD, et al. A phase 3, randomized, controlled trial of resmetirom in NASH with liver fibrosis. N Engl J Med 2024;390:497–509.
[51] Dong XC. FOXO transcription factors in non-alcoholic fatty liver disease. Liver Res 2017;1:168–173.
[52] Liu D, Zhang T, Chen X, et al. Correction to: ONECUT2 facilitates hepatocellular carcinoma metastasis by transcriptionally upregulating FGF2 and ACLY. Cell Death Dis 2021;13:28.
[53] Ao R, Wang Y, Tong J, et al. Altered microRNA-9 expression level is directly correlated with pathogenesis of nonalcoholic fatty liver disease by targeting Onecut2 and SIRT1. Med Sci Monit 2016;22:3804–3819.
[54] Wang S, Li K, Pickholz E, et al. An autocrine signaling circuit in hepatic stellate cells underlies advanced fibrosis in nonalcoholic steatohepatitis. Sci Transl Med 2023;15:eadd3949.

Keywords: liver pathology; fibrosis; diet; carbohydrates; lipids; sex differences.
Received 28 February 2024; received in revised form 12 September 2024; accepted 17 September 2024; Available online 21 September 2024